Hypocretin neuron-specific transcriptome profiling identifies the sleep modulator Kcnh4a

Laura Yelin-Bekerman, Idan Elbaz, Alex Diber, Dvir Dahary, Liron Gibbs-Bar, Shahar Alon, Tali Lerer-Goldshtein, Lior Appelbaum

DOI: http://dx.doi.org/10.7554/eLife.08638

Cite as: eLife 2015;10.7554/eLife.08638

Received: 10 May 2015
Accepted: 30 September 2015
Published: 1 October 2015

Hypocretin neuron-specific transcriptome profiling identifies the sleep modulator Kcnh4a

Laura Yelin-Bekerman[1,2], Idan Elbaz[1,2], Alex Diber[1,2], Dvir Dahary[3], Liron Gibbs-Bar[4], Shahar Alon[5], Tali Lerer-Goldshtein[1,2], Lior Appelbaum[1,2,*]

[1]The Mina and Everard Goodman Faculty of Life Sciences, Bar-Ilan University, Ramat-Gan 5290002, Israel

[2]The Leslie and Susan Gonda Multidisciplinary Brain Research Center, Bar-Ilan University, Ramat-Gan 5290002, Israel

[3]Toldot Genetics Ltd., Hod Hasharon, Israel

[4]Department of Biological Regulation, The Weizmann Institute of Science, Rehovot 7610001, Israel

[5]Media Lab, Massachusetts Institute of Technology, Cambridge, MA 02139, USA

Running Title: Sleep and the transcriptome of Hcrt neurons

*Corresponding author: lior.appelbaum@biu.ac.il

Keywords: hypocretin, orexin, zebrafish, sleep, transcriptome, *kcnh4a*

Abstract

Sleep has been conserved throughout evolution; however, the molecular and neuronal mechanisms of sleep are largely unknown. The hypothalamic hypocretin/orexin (Hcrt) neurons regulate sleep/wake states, feeding, stress, and reward. To elucidate the mechanism that enables these various functions and to identify sleep regulators, we combined fluorescence cell sorting and RNA-seq in *hcrt:EGFP* zebrafish. Dozens of Hcrt-neuron–specific transcripts were identified and comprehensive high-resolution imaging revealed gene-specific localization in all or subsets of Hcrt neurons. Clusters of Hcrt-neuron–specific genes are predicted to be regulated by shared transcription factors. These findings show that Hcrt neurons are heterogeneous and that integrative molecular mechanisms orchestrate their diverse functions. The voltage-gated potassium channel Kcnh4a, which is expressed in all Hcrt neurons, was silenced by the CRISPR-mediated gene inactivation system. The mutant *kcnh4a* (*kcnh4a*$^{-/-}$) larvae showed reduced sleep time and consolidation, specifically during the night, suggesting that Kcnh4a regulates sleep.

Introduction

Sleep is a fundamental behavior that benefits the brain and sleep disorders affect a large portion of the world's population (1). Thus, it is essential to identify and understand the role of the neuronal circuits and genes that regulate sleep. The hypothalamus centralizes sleep regulation and maintains essential physiological processes, including growth, reproduction, body temperature, stress, reward, feeding, and circadian rhythms (2–9). These functions are mediated by several hypothalamic nuclei that interact with various neuronal networks. Some of these nuclei, such as the suprachiasmatic nucleus (SCN), which is the master circadian oscillator (10), have been well characterized both anatomically and physiologically, while the neuronal identity and function of other nuclei is less understood (11–13). The hypocretin (Hcrt, also called orexin) neurons secrete the Hcrt neuropeptides and are located in the lateral hypothalamus (LH). These hypothalamic neurons project to wide areas in the brain, including the tuberomammillary nucleus, paraventricular thalamic nucleus, arcuate nucleus, and monoaminergic nuclei (14). They were initially implicated in feeding behavior and sleep/wake cycles (15,16). Their role in sleep regulation was further strengthened since loss of Hcrt neurons causes the sleep disorder narcolepsy, which is characterized by sleep/wake fragmentation, increased body mass, and cataplexy (loss of muscle tone, often triggered by emotional stimuli) (17–22). However, extensive research showed that the function of Hcrt neurons is much broader and also includes regulation of energy homeostasis, pain, emotion, stress response, and reward (12,14,23). The Hcrt neurons regulate this variety of brain functions through interactions with peptide-secreting neurons and with the monoaminergic, dopaminergic, and limbic systems, among others (24).

How do Hcrt neurons serve as a multifunctional hypothalamic system? Clearly, secretion of the neuropeptide Hcrt is a key pathway. A single *hcrt* gene encodes for the precursor polypeptide prepro-Hcrt, which is cleaved to produce two Hcrt neuropeptides. The actions of the Hcrt neuropeptides are mediated via two Hcrt G-protein–coupled receptors (Hcrtrs) (14). In addition, the synaptic release of glutamate from Hcrt neurons has been shown to affect the activity of post-synaptic target neurons (25,26). However, Hcrt neurons contain additional proteins that are likely involved in mediating their development, plasticity, and diverse functions. To date, only a few Hcrt-neuron–specific genes were substantially characterized and, except for *hcrt*, none of them are exclusively expressed in Hcrt neurons (27–40). A comprehensive and specific gene-expression profiling of Hcrt neurons will enhance the understanding of Hcrt neuronal networks and its diverse functions.

Three studies have described the gene-expression profile of Hcrt neurons in rodents (33,34,36). First, RNA array was used to study the effect of loss of Hcrt neurons on the expression of hypothalamic transcripts in Hcrt-neuron–ablated mice (36). Later, using affinity purification of RNAs and transgenic mice that express FLAG-tagged poly(A)-binding protein, specifically in Hcrt neurons, polyadenylated mRNA was isolated and classified (33). Finally, the translating ribosome affinity purification technique that targets HCRT-producing neurons, was used to isolate Hcrt cell-specific RNA in mice (34). These extensive studies resulted in a list of genes expressed in Hcrt neurons. However, in the opaque mammalian brain, isolation of the entire Hcrt neuron population is challenging because a few thousand Hcrt cells are intermingled with other hypothalamic neurons. In addition, all studies used microarray technology, which limits gene resolution and requires *a priori* knowledge of transcript content.

The zebrafish has become a valuable model for the study of specific neuronal populations in live animals. It is a simple and diurnal vertebrate that combines powerful genetic tools with conserved anatomy and function of the brain (41–43). In the last two decades, behavioral criteria have been used to characterize sleep in zebrafish (44–48). Similar to mammals, the Hcrt neurons are located in the zebrafish hypothalamus but, in contrast to mammals, the zebrafish Hcrt system contains only a few neurons, making it a relatively simple system to study (49,50). Functional studies using Hcrt-neuron–specific genetic ablation, as well as genetic manipulation of the *hcrt* ligand and receptors, showed that the Hcrt system regulates sleep and wake in zebrafish (45,46,48). In addition, the zebrafish Hcrt neurons induce feeding behavior (51), as is the case in mammals. Recently, in order to study Hcrt-neuron specification, a screen for regulatory factors was conducted in the early stages of zebrafish development [26 hours post-fertilization (hpf), (37)]. Similar to mammals (34), microarray gene-expression analysis revealed that the LIM homeobox transcription factor Lhx9, which is widely expressed in the brain, including in the Hcrt neurons, can induce the specification of Hcrt neurons (37). In the present work, we used 7-days-post-fertilization (dpf) transgenic zebrafish larvae expressing EGFP under the promoter of *hcrt* (52), to identify genes that regulate Hcrt-neuron function. The *hcrt:EGFP* larvae were used to specifically isolate Hcrt neurons by fluorescence-activated cell sorting (FACS). Using whole transcriptome RNA sequencing (RNA-seq), meticulous bioinformatic analysis, and extensive anatomical validations, a novel set of Hcrt-neuron–specific genes was identified. Furthermore, the role of the voltage-gated potassium channel Kcnh4a in regulating sleep architecture was studied.

Results

Isolation of Hcrt neurons

In order to isolate the Hcrt neurons, the transgenic *hcrt:EGFP* zebrafish (52), which enables specific visualization and manipulation of the entire population of Hcrt neurons (16-20 cells per larva), was used. At 7 dpf, the heads of *hcrt:EGFP* larvae (Figure 1A-B) were dissociated, and EGFP-positive ($EGFP^+$) cells from the cell suspension sample (Figure 1C) were sorted by FACS (Figure 1D-G). The sorting thresholds were set to accurately detect the small amounts of cells expressing EGFP while avoiding the auto-fluorescent cells derived primarily from the eyes of the larvae (Figure 1B). In order to calibrate the threshold and additional FACS parameters, *α-tubulin:EGFP*-injected larvae (Figure 1E), which expressed EGFP in the entire central nervous system (CNS), were also FAC-sorted. To avoid off-target sorting of EGFP-negative ($EGFP^-$) cells and to set the threshold of $EGFP^+$ cells, we applied the same parameters and filters to a cell suspension sample derived from wild-type (WT) larvae (Figure 1F). As expected, the number of $EGFP^+$ cells sorted from *hcrt:EGFP* larvae (Figure 1G) was low compared with the number of cells sorted from *α-tubulin:EGFP*-injected larvae. $EGFP^+$ cells were not detected in WT larvae (Figure 1F). Using this technique, we collected 300 $EGFP^+$ and 300 $EGFP^-$ cells from *hcrt:EGFP* larvae in three independent experiments. To verify that the $EGFP^+$ cells were Hcrt neurons, RNA extraction was performed, followed by reverse transcription PCR (RT-PCR) assays. While *hcrt* and *egfp* were detected in $EGFP^+$ cells, they were not amplified in $EGFP^-$ cells (Figure 1H). These results show that the $EGFP^+$ cells mostly contain Hcrt neurons, while the $EGFP^-$ group contains a heterogeneous population of cells from the whole larva head. Since the amount of RNA extracted from 300 cells was extremely low (below 1 pg/µl) and required pre-amplification before deep sequencing, RNA was extracted from a third control group

of cells derived from a whole head of 7 dpf WT larvae. This group helped to distinguish false positive signals that might have resulted from the amplification, and covered genes that were widely expressed in the head and not restricted to 300 $EGFP^-$ cells. The RNA of the three groups: $EGFP^+$, $EGFP^-$, and whole head, was subjected to RNA-Seq and bioinformatic analysis (Figure 1I) to obtain a list of Hcrt-neuron–enriched genes.

Systematic identification and spatial characterization of genes enriched in Hcrt neurons

We aimed to identify novel players that regulate the myriad of processes coordinated by Hcrt neurons. Thus, the RNA-seq data from $EGFP^+$, $EGFP^-$, and whole-head groups (http://www.ncbi.nlm.nih.gov/sra, PRJNA283169) were analyzed *in silico*. Initially, the raw read counts were normalized to transcripts per million (TPM), and a gene was considered to be preferentially expressed in the Hcrt cells only if its normalized expression level was at least 100 TPM in $EGFP^+$ cells. In addition, the expression levels were required to be at least 7 times more abundant in the $EGFP^+$ than in both controls. These criteria stipulated a high level of specificity to the $EGFP^+$ samples relative to the control samples. The bioinformatic analysis identified 20 transcripts that were found to meet these criteria ($p<0.01$, Figure 2A). Among the 20 transcripts, 12 were annotated genes and 8 were non-annotated transcripts. Notably, the *hcrt* gene was expressed at a level of 300 TPM in $EGFP^+$ and below 10 TPM in both control samples. The identification of an *hcrt* gene confirmed the specificity of the cell sorting, the RNA-seq, and the bioinformatic analysis.

In order to validate the bioinformatic results and to determine the spatial expression pattern of the candidate genes, whole-mount *in situ* hybridization (ISH) was performed on 2 dpf WT larvae (Figure 2B-M) using gene-specific probes for the enriched genes (Figure 2A). Nine of them were found to be expressed in the hypothalamic area (*hcrt*, *star*, *dennd1b*, *kcnh4a*, *fam46a*, *si:dkey-58b18.8*, *cuff23873.1*, *npvf*, and *npffr*; Figure 2B-M). Five transcripts (*adra*, *ptgs2b*, *grpr*, *cuff64723*, and *cuff77494,*) could not be amplified, and the expression of six transcripts (*elovl7b*, *cuff34876*, *cuff70256*, *cuff442204*, *cuff57637*, and *cuff77484*) was not detected at the 2 dpf larval stage. To test whether these genes were expressed in later developmental stages, their expression was studied in adults. However, only *elovl7*b showed a detectable expression in the hypothalamus (Figure 3J-J''). The hypothalamic expression pattern of the candidate genes was similar to the expression pattern of *hcrt* (Figure 2B), suggesting that the candidate genes may be expressed in Hcrt neurons.

The high percentage of genes that showed hypothalamic expression hints at significant efficiency of the FACS and RNA-seq experiments. Thus, in order to find more Hcrt-neuron–specific genes, we relaxed the bioinformatic parameters to 10 TPM and 3.6 times higher abundance in $EGFP^+$ cells than in the control groups. This analysis revealed 212 transcripts that met the criteria ($p<0.01$, Figure 2–source data 1), among them, 146 were non-annotated (called *cuff*-serial number) and 66 were annotated genes. The functional roles of the annotated genes are diverse and include, for example, regulation of metabolism [such as ELOVL fatty acid elongase 7b (*elovl7*b)], sleep (*lhx9*), synaptogenesis and synaptic plasticity [such as the guanine nucleotide exchange gene (*denndbl*)]. Some of the non-annotated transcripts were likely long, non-coding RNA (lncRNA) since they were longer than

200 bp, did not include a coding sequence, and were located in intergenic regions (53). lncRNAs regulate transcription and epigenetic processes and may be involved in the regulation of splicing and translation (54). Notably, some non-annotated transcripts were located in the zebrafish genome near Hcrt-enriched genes. In addition to the 8 genes tested (Figure 2C-J), we attempted to examine the expression of selected candidate genes that demonstrate relatively lower enrichment in Hcrt neurons (Figure 2–source data 1). We selected *zgc:171844,* H6 homeobox 3 (*hmx3*), and *lhx9*, which were located in the bottom 100 genes in the list (Figure 2–source data 1). Previous work showed that *lhx9* is expressed in Hcrt neurons in mammals and zebrafish (34,37) and that *hmx3* is expressed in Hcrt neurons in the early stages of zebrafish development (37). Similar to the genes that demonstrated high fold change (Figure 2A), these three genes were also expressed in the hypothalamus, where *hcrt* is expressed (Figure 2K-M), suggesting that a large portion of the 212 transcripts (Figure 2–source data 1) may be expressed in the Hcrt neurons.

Identification of genes localized in Hcrt neurons

Single-probe ISH analysis showed that selected candidate transcripts are expressed in the hypothalamus and that their spatial expression pattern is reminiscent of the expression of the *hcrt* gene (Figure 2). To test whether these transcripts are expressed in Hcrt neurons, we performed whole-mount fluorescent ISH using probes for the candidate genes, coupled with immunofluorescence staining using EGFP antibody, in *hcrt:EGFP* 2 dpf larvae and adults. To verify the efficiency and specificity of this assay, co-localization of *hcrt* and EGFP was initially confirmed (Figure 3A-A''). Double staining showed that among the 11 transcripts tested, 8 transcripts (*star*, *dennd1b*, *kcnh4a*, *fam46a*, *hmx3*, *zgc171844*, *lhx9*, and *si:dkey-*

58b18.8) co-localized with EGFP in Hcrt neurons (Figure 3B-I"). While *kcnh4a*, *hmx3*, *lhx9* and *dennd1b* were expressed in most Hcrt neurons, *star*, *fam46a*, and *zgc171844*, were expressed in a subset of the Hcrt neurons. In addition to their expression in Hcrt neurons, these transcripts were also expressed in other brain regions, particularly other hypothalamic areas and the forebrain. In contrast, *si:dkey-58b18.*8 demonstrated relatively weak expression that was predominantly apparent in Hcrt neurons (Figure 3E-E"). Further anatomical analysis in *hcrt:EGFP* adult brain sections was performed on four transcripts (Figure 3J-M"): *elovl7b*, which did not show expression in the earlier developmental stages (Figure 3J-J"), *kcnh4a* (Figure 3K-K"), *dennd1b* (Figure 3L-L"), and *zgc171844* (Figure 3M-M"). Double staining in adults showed that *kcnh4a* and *elovl7b* are detected in all Hcrt neurons, while *dennd1b* is expressed in about half of the Hcrt neurons and *zgc171844* in about a third of the neurons. Notably, the portion of co-localization with EGFP in larvae was similar to that in adults. Altogether, the anatomical results validated the RNA-seq and bioinformatic analysis, which provide a comprehensive list of Hcrt neuron-specific transcripts. The spatial expression of these transcripts in subpopulations of Hcrt neurons indicates that Hcrt neurons are not a uniform population but rather heterogeneous neurons. Understanding the function of these transcripts will provide the basis to elucidate the mechanism that regulates the multifunctions of Hcrt neurons.

Identification of hypothalamic neuronal populations located adjacent to Hcrt neurons

The histochemical assays revealed transcripts expressed in Hcrt neurons. However, three candidate transcripts (*cuff.23873*, *npvf*, and *npffr*; Figure 2H-J*)* labeled distinct

hypothalamic populations of neurons that intermingled with Hcrt neurons, but co-localization was not detected (Figure 4). These cell populations were located in the immediate vicinity of the Hcrt neurons in the hypothalamus. While, *cufff.23873* (Figure 4A-C") and *npffr* (Figure 4D-F") were also expressed in the forebrain area, *npvf* (Figure 4G-I") showed a specific hypothalamic expression pattern. The finding of transcripts that were apparently not expressed in Hcrt neurons in the transcriptome, could be due to the adhesion of hypothalamic cells adjacent to Hcrt neurons during the FACS procedure, or because these transcripts are also expressed by Hcrt neurons but below ISH detection levels. Nonetheless, these transcripts are predominantly expressed in hypothalamic neurons and may interact with Hcrt neurons to form neuronal networks that mediate the functions of Hcrt neurons.

Hcrt-neuron–specific genes are predicted to share similar transcription regulation

The mechanism that regulates the specific expression of transcripts in Hcrt neurons and the identity of the transcription factors (TFs) is unclear. To identify candidate TFs that can regulate multiple Hcrt-neuron–specific genes, a map of possible TF binding sites was generated based on the 48 most enriched transcripts. Conserved sequences in the predicted regulatory region of each Hcrt-neuron–specific gene were characterized, and the matched TFs that potentially bind to these sequences were identified. This analysis revealed 68 putative TFs (Figure 5A and Figure 5–source data 1), among them, 13 showed significant enrichment in the top 48 Hcrt-specific transcripts (p<0.005, Figure 5A) including *nr6a1*, which is a regulator of *hcrt* in mice (55). Notably, this analysis suggests that several specific TFs regulate numerous Hcrt-neuron–specific genes (Figure 5A). For example, the heat shock

transcription factor 1 (*hsf1*) is predicted to regulate 25 Hcrt-neuron–enriched genes: *hcrt*, *ptgs2*, *ttn*, *hspa1l*, *grpr*, *elovl7b*, *slc4a1*, *lhx9*, *c16orf45*, *soat2*, *tsen54*, *nos1*, *rfx4*, *syt10*, *trpc7*, *ntng1, cacng4*, *myh4*, *dennd1b*, *sgsm1*, *pde2a*, *wscd1*, *adra1a*, *kcnh4a*, and *hmx3*. To test whether this predicted TF is expressed in Hcrt neurons, fluorescent ISH, using a probe for *hsf1,* and fluorescent immunostaining using an antibody against EGFP, were performed on the brain section of adult *hcrt:EGFP* zebrafish (Figure 5B-C"). This assay showed wide brain expression of *hsf1* and confirmed that *hsf1* is also expressed in Hcrt neurons. In mammals, *hsf1* is a key activator of stress conditions, and the Hsf1 null mice showed major brain morphological alterations (56). In zebrafish, *hsf1* is essential for recovery from ischemic injury in the brain (57). In addition to *hsf1*, the TF binding-site analysis revealed the enrichment of TFs that regulate metabolic processes (*pax4*, *hnf1*, *ppara*, *lhx3*, *creb*, and *foxo4*), such as control of the levels of glucagon, insulin, somatostatin, lipids, and glucose (58–63). In addition, *ap-2*, a TF that is required for sleep-like behavior in *C. elegans* (64), was predicted to regulate the transcription of 13 Hcrt neuron-specific genes (Figure 5A). The identification of mutual TF binding sites in the regulatory sequences of Hcrt-neuron–specific genes suggests that several key TFs regulate the development and function of Hcrt neurons.

Synteny, cloning, and protein structure of Kcnh4a

Among the candidate genes (Figure 2–source data 1), the voltage-gated potassium channel *kcnh4a* was of particular interest because of its genomic location, expression pattern, and predicted role. Two *kcnh4* are present in zebrafish: *kcnh4a* (KR733682) located in chromosome 3 and *kcnh4b* (XM_690738) located in chromosome 12. In contrast to the broad expression of *kcnh4b* (data not shown),

kcnh4a is expressed specifically in the forebrain and hypothalamus in larvae (Figure 2E). Double ISH and immunofluorescence staining revealed that *kcnh4a* is localized in all Hcrt neurons in both larvae and adults (Figure 3D-D" K-K") and like Hcrt neurons, hypothalamic *kcnh4a*-expressing neurons are glutamatergic (Figure 6–figure supplement 1). Intriguingly, *kcnh4a* is localized only a few kilobase pairs (kbp) downstream to *hcrt* on the genome, and a synteny analysis showed that the genomic organization of this locus is conserved with mammals (Figure 6A). In humans, *kcnh4a* is located only 3782 bp downstream to the *hcrt* gene, while in zebrafish, the distance between the genes is 5517 bp (Figure 6A). Although *kcnh4a* expression is not restricted to Hcrt neurons, the genomic proximity of the two genes suggests a mutual transcription regulation. Indeed, a significant portion of the TFs predicted to regulate *hcrt* can also bind to *kcnh4a* regulatory sequences (48 out of 52, Figure 5–source data 1).

Vector cloning and sequencing of *kcnh4a* showed that the gene consists of 16 exons, which include the 3456 bp coding sequence (CDS, Figure 6B). The start codon is located within the second exon, preceded by 1884 bp 5' UTR. Exon 16 includes the stop codon, followed by 1286 bp 3'UTR. Structural bioinformatic analysis of the protein sequence revealed that the Kcnh4a contains the evolutionarily conserved six S domains that characterize the potassium voltage-gated ion channels (Figure 6B) (65). Domains S1-S4 constitute the voltage-gated domain that senses changes in membrane potential (66,67), whereas domains S5-S6 form the selectivity pore through which ions can flux (65–67). Next, phylogenetic analysis revealed that the zebrafish Kcnh4a protein is evolutionarily conserved with vertebrate orthologs (68). As expected, the zebrafish Kcnh4a protein showed the

highest homology to the Kcnh4 of another fish (*Larimichthys_crocea*) and, to a lesser extent, to the mammal Kcnh4 proteins (Figure 6C).

Mild, reduced locomotor activity in *kcnh4a*$^{-/-}$ larvae

In order to test the function of Kcnh4a, we established a clustered, regularly interspaced, short palindromic-repeat (CRISPR)-based *kcnh4a* mutant zebrafish (*kcnh4a* $^{-/-}$). A 14 bp deletion mutation was generated in exon 5, which encoded part of the pore domain. This deletion introduced a premature stop codon and is predicted to result in truncated protein (Figure 6D). Furthermore, quantitative reverse transcription PCR (qRT-PCR) showed a reduction of 59% of *kcnh4a* mRNA levels in *kcnh4a* $^{-/-}$ compared to WT-sibling (*kcnh4a*$^{+/+}$) 6dpf larvae (p<0.001, Figure 6E). The founder (F0) fish was outcrossed with WT fish, and experiments were performed on the progeny of inter-crosses between F4 heterozygous fish (*kcnh4a*$^{+/-}$).

To study the rhythmic locomotor activity of *kcnh4a*$^{-/-}$ zebrafish, high-throughput video-tracking systems were used (48). The locomotor activity of *kcnh4a*$^{-/-}$ (n=85), *kcnh4a*$^{+/-}$ (n=209), and *kcnh4a*$^{+/+}$ (n=98) was monitored during day and night (14 h light/10 h dark). As expected, larvae from all three genotypes exhibited rhythmic locomotor activity that peaked during the day ($F_{[2,180]}$=14.98; p<0.0001, mixed-effect model with repeated measures; Figure 7A). Notably, *kcnh4a*$^{-/-}$ larvae were slightly hyperactive (average: 13.84 ± 0.11) compared to *kcnh4a*$^{+/-}$ (average: 13.29 ± 0.07, t=-4.19, df=180, p<0.01) and *kcnh4a*$^{+/+}$ sibling larvae during the day (average: 12.98 ± 0.1, t=5.73, df=180, p<0.0001). During the night, the differences in locomotor activity were even lower, and the *kcnh4a*$^{-/-}$ larvae were slightly more active (average: 8.05 ± 0.13) than the *kcnh4a*$^{+/+}$ larvae (average: 7.64 ± 0.12, t=2.28, df=180, p<0.05;

Figure 7A, 7B). These results show that the loss of Kcnh4a mildly increases larval locomotor activity, particularly during the day.

Reduced sleep time and altered sleep architecture in *kcnh4a*$^{-/-}$ larvae during the night

Similar to humans, the zebrafish is a diurnal vertebrate that sleeps during the night (69,70). Using well-established behavioral criteria, sleep in larvae was defined as a period of one or more minutes of immobility, which is associated with an increase in arousal threshold (45,48). A previous study has shown that six hours of sleep deprivation (SD) during the night reduced locomotor activity in the following day (44). Similarly, six hours of SD during the night increased sleep time during the following day in 6 dpf larvae (Figure 7–figure supplement 1). Thus, similar to mammals, sleep in zebrafish larvae is regulated by circadian and homeostatic processes.

Voltage-gated potassium channels are activated by membrane depolarization and contribute to neuronal repolarization and repetitive firing (71). Considering this role and the expression of *kcnh4a* in all Hcrt neurons, we tested whether it regulates sleep and wake. Similar to humans, zebrafish are diurnal animals; thus, all three genotypes (*kcnh4a*$^{-/-}$, *kcnh4a*$^{+/-}$, and *kcnh4a*$^{+/+}$) slept more during the night than during the day ($F_{[2,180]}$=14.52; p<0.0001, mixed-effect model with repeated measures, Figure 7C). Remarkably, while the amount of sleep was similar in all genotypes during the day (average: *kcnh4a*$^{-/-}$= 2.76 ± 0.22; *kcnh4a*$^{+/-}$= 2.80 ± 0.14; and *kcnh4a*$^{+/+}$= 2.87 ± 0.21), sleep time was reduced in *kcnh4a*$^{-/-}$ larvae compared with *kcnh4a*$^{+/-}$ and *kcnh4a*$^{+/+}$ larvae during the night (average: *kcnh4a*$^{-/-}$= 13.08 ± 0.27; *kcnh4a*$^{+/-}$= 14.78 ± 0.17; and *kcnh4a*$^{+/+}$= 15.46 ± 0.25, t=-6.55, *df*=180,

p<0.0001, Figure 7C, 7D). In order to examine the sleep architecture, we quantified the number of sleep/wake transitions and the length of sleep bouts. While the number of sleep/wake transitions did not change during the day (*kcnh4a*$^{-/-}$= 3.52 ± 0.16; *kcnh4a*$^{+/+}$= 3.79 ± 0.15), their number was decreased in *kcnh4a*$^{-/-}$ larvae during the night (average: *kcnh4a*$^{-/-}$= 12.68 ± 0.19; *kcnh4a*$^{+/+}$= 13.62 ± 0.18, transitions/hour, $F_{[1,80]}$=13.16; *p*<0.0005; *df*=80, *p*<0.0005, Figure 7E). In addition, the *kcnh4a*$^{-/-}$ larvae exhibit shorter sleep-bout length specifically during the night (average: *kcnh4a*$^{-/-}$= 2.21 ± 0.05; *kcnh4a*$^{+/+}$= 2.43 ± 0.05; min\hour *df*=81, *p*<0.005, Figure 7F). Thus, the reduction in the number and length of sleep episodes causes global reduction in sleep time during the night in *kcnh4a*$^{-/-}$ larvae. These results show that the loss of Kcnh4a affects sleep time and sleep consolidation, specifically during the night. It also suggests that Kcnh4a regulates sleep by repolarization of the membrane potential in sleep-regulating neurons.

Discussion

How the hypothalamic Hcrt neurons regulate diverse and fundamental physiological functions and what is the molecular mechanism that controls sleep are largely open questions. We revealed the molecular profile of the Hcrt neurons and functionally demonstrated the role of Kcnh4a in regulating sleep. Using FAC-sorting of the whole Hcrt neuronal population and RNA-seq of minute amounts of RNA, 212 Hcrt-neuron–specific transcripts were identified. Combination of fluorescent ISH and immunofluorescence assays confirmed that several transcripts are expressed in Hcrt neurons. The high efficiency and specificity of these anatomical experiments suggest that a large portion of the candidate genes (Figure 2–source data 1) are expressed in Hcrt neurons. Indeed, *lhx9* and *hmx3*, which were ranked lower in the

list of candidate genes, were previously shown to be expressed in the early stages of Hcrt-neuron development (34,37), and we confirmed these observations in 7 dpf larvae. Thus, these results provide a comprehensive list of genes that are likely to mediate the multifunctions of Hcrt neurons. Comparison between the Hcrt-neuron–specific candidate genes isolated in zebrafish and mice (34) showed that eight genes (*rfx4*, *lhx9*, *scg2*, *vgll2*, *ptprn*, *creb3l1*, *sgsm1*, and *fam46a*) are found in both vertebrates. This genetic similarity is reasonable; however, performing similar cell isolation technique and bioinformatic analysis in both species would have likely increased the list of shared Hcrt-neuron–specific genes. Accumulated data on mammals and zebrafish suggest that the Hcrt neurons are not a homogenous population (27,34). Indeed, our co-localization studies showed a diversity of spatial gene expression in Hcrt neurons, varying from partial to complete overlapping with *hcrt*. Thus, the molecular signature suggests that these neurons are divided into subpopulations that may cope with the wide variety of functions of Hcrt neurons. The development and diverse functions of Hcrt neuron subpopulations are predicted to be regulated by Hcrt-neuron–expressed TFs, which target an ensemble of Hcrt-neuron–specific genes.

The role of the isolated Hcrt-neuron–specific genes is diverse. Large arrays of genes are involved in the regulation of metabolism, endocrine systems, synaptic function, neurogenesis, reward, wake, and sleep (Figure 2–source data 1). These functions are correlated with the diverse role of Hcrt neurons. A group of genes includes metabolic and endocrine genes, such as the protein tyrosine phosphatase receptor (*ptprn*), which is implicated in insulin regulation (72,73), and the steroidogenic acute regulatory protein (*star*), which regulates the production of steroid hormones from cholesterol in the mitochondria (74–76). Another gene

involved in metabolism is *elovl7*b, which regulates fatty acid metabolism and energy homeostasis. This gene has been linked to lipodystrophy, obesity, and other metabolic disturbances (77,78). These metabolic genes are likely part of the mechanism that regulates feeding and obesity. Thus, in addition to *hcrt*, an imbalance of the fatty acid and glucose-regulating genes and pathways may contribute to the metabolism-related symptoms of narcoleptic patients.

An array of Hcrt-neuron–specific genes are involved in neurogenesis and synaptic plasticity. For instance, the synaptic vesicle protein synaptotagmin X (*syt10*), which is involved in vesicular trafficking and Ca(2+)-dependent exocytosis (79,80). In addition, the voltage-dependent calcium-channel (*cacgn4*) gene regulates the biophysical properties of α-amino-3-hydroxy-5-methyl-4-isoxazolepropionic acid (AMPA) receptors (81) and secretogranin II (*scg2*) encodes to a secretory protein and mediates the packaging and sorting of neuropeptides into secretory vesicles (82,83). Additional examples include the *denndbl*, which is involved in axon guidance, synaptic plasticity, and synaptic vesicle exocytosis (84), and netrin G1 (*ntng1*), which is part of the mechanism that regulates axon guidance during development (85,86). Altogether, these genes are likely to play a key role in the mechanism that regulates neuritic processes, synaptic plasticity and activity in Hcrt neurons.

In addition to annotated genes, the RNA profiling also revealed a set of long, non-coding RNA (lncRNAs) enriched in Hcrt neurons. lncRNAs regulate gene transcription and expression via various molecular mechanisms. Several studies show that lncRNAs regulate the expression of protein-coding genes, with their genomic loci adjacent to the locus of the specific lncRNA (54,87). Supporting these

observations, among the 16 lncRNAs that were enriched in Hcrt neurons, several were located in the genome next to the Hcrt-neuron–specific genes. For instance, the lncRNA *cuff23873* is placed between the genes *hacl1* and *ankrd28* while *si:dkey-58b18.8* is located in the intergenic region between *pim2* and *rpp40*. Thus, these results suggest that Hcrt-neuron–specific lncRNAs regulate transcriptional and post-transcriptional processes of Hcrt-neuron–specific genes.

The identification of hundreds of Hcrt-neuron–specific candidate genes enabled us to predict the TFs that regulate the expression of these genes. We found a significant enrichment of TFs, which regulate metabolism, sleep, and other physiological processes (Figure 5). For example, the hepatic nuclear factor 1 homeobox (*hnf1*) regulates the expression of genes involved in lipid and glucose transport (62). In the Hcrt neurons, it was expected to regulate 35 out of the 48 Hcrt-neuron–specific genes (Figure 5), including five metabolic genes (*soat2*, *f2rl1*, *scg2*, *grpr*, and *elovl7*b). Another key TF is the peroxisome proliferator-activated receptor alpha (*ppara*), which plays a role in lipid metabolism and satiety (58,59). In the Hcrt neurons, this TF is expected to regulate the transcription of 33 Hcrt-neuron–specific genes, such as *ptprn*, *soat2*, *f2rl1*, *scg2*, and *grpr*, which are associated with the balancing of metabolism. Notably, the TF *ap1*, which is associated with sleep induction (64), is expected to be a regulator of 13 Hcrt-neuron–specific genes, including *lhx9*, which regulates sleep (34). Intriguingly, *ap1* can also regulate the expression of Hcrt-neuron–specific synaptic genes, such as *cacgn4*, *nos1*, and *dennd1b*. Since sleep regulates synaptic plasticity in Hcrt axons (28), *ap1* might mediate the molecular mechanism that links sleep with synaptic plasticity in Hcrt neurons.

The different players that are expressed in Hcrt neurons modulate the diverse roles of the neurons; however, these functions are also mediated by other hypothalamic neuronal networks. Aside from the Hcrt-neuron–specific genes, we identified three transcripts, *cuff8731*, *npvf,* and *npffr1*, which are expressed in cells located adjacent to Hcrt neurons. The neuropeptide VF precursor (*npvf*) and its receptor (*npffr1*) regulate nociception, anxiety, learning, and memory (88). The NPVF/NPFFR1 system also controls pain and analgesia through interactions with the opioid system (88). The opioid system is formed, among others, by Nociceptin that forms the nociceptin/orphanin FQ (N/OFQ) system. This system makes synaptic contacts with Hcrt neurons, inhibiting their activity via pre- and post-synaptic mechanisms. The nociceptin/orphanin FQ (N/OFQ) system also exerts diverse actions in the hypothalamic–pituitary–adrenal (HPA) axis, and is implicated in the neurobiological control of stress and associated adaptive behaviors (89). More specifically, Hcrt neurons are essential in the generation of stress-induced analgesia (SIA), and N/OFQ blocks SIA via inhibition of Hcrt neuron activity (90). Altogether, NPVF/NPFFR and Hcrt neurons may interact in the hypothalamus to regulate morphine- and stress-induced analgesia.

Among the candidate Hcrt-neuron–specific genes, we studied the role of *kcnh4a*, which is located adjacent to *hcrt* in the genome and is expressed in all Hcrt neurons. We found that sleep time, sleep/wake transitions, and sleep-bout length are decreased in *kcnh4a*$^{-/-}$ larvae during the night. Since potassium voltage-gated channels repolarize the cell membrane (65–67), loss of *kcnh4a* may reduce potassium efflux and induce repetitive hyperpolarization, and, ultimately, nighttime wakefulness. Supporting this role, the ether-a-go-go-gene–related (ERG) potassium channel blockers selectively increased waking activity at night in zebrafish (91). The

importance of potassium channels for sleep regulation has also been demonstrated in flies. Genetic screen of fly mutants revealed the short sleeper *shaker* mutant. The *shaker* gene encodes a voltage-dependent potassium channel and regulates sleep need and efficiency (92). Notably, loss of the *shaker* and *kcnh4a* potassium channels similarly affects nighttime sleep, while daytime sleep is unaffected in *kcnh4a*$^{-/-}$ larvae. In mice, loss of the voltage-dependent potassium channel Kcna2 decreases non-rapid-eye-movement (NREM) sleep and increases wakefulness (93). These findings suggest that sleep is regulated by neuronal-circuit–specific potassium channels in flies, zebrafish, and mammals. According to this model, in zebrafish, the presence of Kcnh4a in the excitatory Hcrt neurons suggests that Kcnh4a regulates their activity and, ultimately, sleep and wake. In *kcnh4a*$^{-/-}$ larvae, the absence of Kcnh4a may cause hyperexcitability of the Hcrt neurons that induces the activity of downstream arousal-promoting targets, such as the paraventricular thalamic nucleus (94) and the locus coeruleus (95). However, since the expression of Kcnh4a is not restricted to Hcrt neurons and its effect on firing rates in specific neuronal population is not clear, further neurophysiological studies are required to link Kcnh4a, neuronal activity, sleep and wakefulness.

The Hcrt transcriptome identified Kcnh4a as a sleep regulator and provides a platform for future studies on the molecular mechanism that regulates Hcrt-neuron–dependent physiological processes, such as feeding and sleep-wake cycles. In addition, it may also help to identify Hcrt-neuron–specific antigens that trigger the autoimmune response, leading to the specific elimination of Hcrt neurons in narcolepsy (96). Since the transparent zebrafish offer a wide array of tools to manipulate genes and visualize neuronal-circuit activity in live animals, a future combination of CRISPR-mediated mutants, genetically encoded Ca^{+2} indicators, and

optogenetic tools are expected to elucidate the functional role of the Hcrt-neuron–specific genes in a neuronal-circuit–specific manner. These experiments will facilitate our understanding of the mechanism controlling the multifunctional Hcrt neurons.

Methods

Fish Maintenance. The *hcrt:EGFP*, *kcnh4a*$^{-/-}$, *kcnh4a*$^{+/-}$, *kcnh4a*$^{+/+}$, and WT fish were kept in a fish facility under a 14-h light/10-h dark cycle (LD) at 28^{o}C (48) under optimal maintenance conditions, in accordance with the animal protocol approved by the Bar-Ilan University Bioethics Committee. Larvae were generated by paired mating, and raised in incubators and larvae water systems (48) under LD.

FAC-sorting. The heads of 7 dpf *hcrt:*EGFP, *α-tubulin*:*EGFP*-injected, and WT larvae (60 larvae per group) were collected in a 2-ml tube. Cells were then dissociated using the Papain Dissociation System (Worthington Biochemical Corporation, Lakewood, NJ) according to the manufacturer's protocol. The cells were filtered with a 70-μm cell strainer (BD Transduction Laboratories, San Jose, CA) and washed twice with cold phosphate-buffered saline (PBS). High-speed FACS was performed using an LSRII FACS machine (BD, Bioscience, San Jose, CA). A two-gate FACS technique was used to select only EGFP^{+} cells from non-fluorescent and auto-fluorescent cells. The EGFP^{+} cells were differentiated using SSC-A and FSC-A strategies. As a control, two additional groups of cells were sorted: the first group contained only EGFP^{+} cells derived from the heads of larvae expressing *α-tubulin*:EGFP, and the second group contained only EGFP^{-} cells

derived from WT larvae. Then, to separate the EFGP$^+$ cells from the EGFP$^-$ cells, PE-Cy5-A and GFP-A filters were applied. The cells were collected into a 96-well sterile plate filled with the first RNA purification buffer from the RNeasy Mini Kit (Qiagen, Redwood City, CA). The samples were stored at -80^{o}C until the RNA was purified. Three independent FACS experiments were performed, yielding three samples of EGFP$^+$ cells (group 1) and three samples of EGFP$^-$ cells (group 2). Each sample contained 300 sorted cells.

RNA extraction. Six samples (three EGFP$^+$ and three EGFP$^-$) were used for total RNA extraction using the RNeasy Mini Kit (Qiagen, Redwood City, CA) according to manufacturer's protocol. Additionally, total RNA from six samples of the whole head of WT larvae (group 3) was purified using the same kit. Each sample contained 60 heads. The quality and quantity of each RNA sample were assessed by Agilent's 2100 Bioanalyzer 6000 Pico Kit (Agilent Technologies, Santa Clara, CA).

cDNA synthesis and amplification. RNA of group 1 and 2 (Figure 1I) was amplified using the Ovation® RNA-Seq System V2 (NuGEN, San Carlos, CA). Before amplification, all samples were lyophilized using a SpeedVac instrument and then suspended in 5 µl of nuclease-free water. The cDNAs were fragmented using a Bioruptor instrument with three 10-sec ('on') cycles of sonication interrupted by 90-sec pause periods ('off'). The cDNAs of group 3 (Figure 1I) was synthesized according to standard procedures. The cDNAs were quantified using the Nanodrop and Bioanalyzer DNA 1000 Chip. The libraries were loaded on a High Sensitivity ChIP and quantified on a Qubit instrument.

Illumina sequencing and bioinformatic analysis. Illumina TruSeq protocol was used to prepare libraries from RNA samples. Twelve libraries (group 1, 2, 3, Figure 1I) were run on 2 lanes of an Illumina HiSeq2000 machine using the multiplexing strategy of the TruSeq protocol (Institute of Applied Genomics, Udine, Italy). An average of 24 million reads were obtained from $EGFP^+$ RNA, 22 million reads from $EGFP^-$ RNA, and 175 million reads from the whole head RNA (http://www.ncbi.nlm.nih.gov/sra, PRJNA283169). Because of the difference in the amounts of RNA and the amplification process, the reads were 2×50 base pairs for the $EGFP^+$ and $EGFP^-$ groups, and 2×100 for whole larva head groups. The RNA-seq data from the replicates were unified, obtaining three groups for further analysis: $EGFP^+$, $EGFP^-$, and whole head groups. Since the amount of cells and RNA was very low, this strategy increased the read cover for each gene and resolved potential amplification bias. Cufflinks and Cuffdiffs (http://cufflinks.cbcb.umd.edu/) (97,98) were used to calculate gene-expression levels and identify differentially expressed transcripts (statistical analysis is described below). The reads were mapped to the zebrafish genome (Zv9), and raw read counts were normalized to TPM. Initially, a gene was considered to be preferentially expressed in the Hcrt cells if its normalized expression level was at least 100 TPM in $EGFP^+$ cells and 7-fold higher than the higher of the normalized expression levels estimated in the two controls. For reference, the *hcrt*, which was expressed at a level above 300 TPM in the $EGFP^+$ sample and below 10 TPM in the control samples, was used for aligning the reads against the zebrafish genome, allowing only uniquely aligned reads. In order to enlarge the list of enriched transcripts in Hcrt neurons, relaxed parameters were set and the new requirements

were 10 TPM and 3.6 times higher abundance in EGFP^{+} cells compared with the control groups.

Gene ontology analysis and prediction of transcription factors. Following analysis of the RNA-seq data, transcripts that were enriched in Hcrt neurons were either assigned to an annotated zebrafish gene or regarded as novel transcripts. To further characterize the annotated genes, they were assigned a human ortholog using the 'Non-Zebrafish RefSeq Genes' or the 'Human Proteins Mapped by Chained tBLASTn' tracks on the UCSC genome browser (Zv9/danRer7 assembly; http://genome.ucsc.edu/). To find over-represented molecular functions, human orthologs were used as input to DAVID annotation. We focused on over-represented TFs. The DAVID default human-gene background was used. All the significantly enriched (Benjamini-Hochberg adjusted $p<0.05$) TFs are presented in Figure 5–source data 1. The conserved location of transcription factor binding sites was identified in mammalian alignments. A binding site was considered to be conserved across the alignment if its score met the threshold score for its binding matrix. The score and threshold were calculated using the Transfac Matrix Database (v7.0) created by Biobase (Waltham, MA).

Real-time quantitative PCR. The expression levels of *kcnh4a* mRNA were determined using quantitative real-time PCR. Total mRNA was extracted from *kcnh4a*$^{-/-}$ (n=9 batches of 8 larvae) and *kcnh4a*$^{+/+}$ (n=5 batches of 8 larvae) 6 dpf larvae, using the RNeasy Protect Mini Kit (Qiagen, Redwood City, CA) and according to the manufacturer's instructions. A similar amount of mRNA (1µg) was

reverse-transcribed using Oligo(dT) oligos and SuperScript III reverse transcriptase (Invitrogen, Carlsbad, CA) according to the manufacturer's protocol. Transcript levels were determined by Applied Biosystems 7900HT Fast Real-Time PCR System using the Quanta SYBR FAST qPCR Kit (Quanta Biosciences, Gaithersburg, MD). *Ef1a* was used as reference gene (99) and $\Delta\Delta C_T$ analysis was performed (100).

PCR amplification and cloning of candidate genes. To prepare probes for whole-mount ISH experiments, the full coding sequences of the following genes were amplified: *hcrt* (NM_001077392.2), *star* (NM_131663.1), *dennd1b* (XM_009296374.1), *kcnh4a* (KR733682), *fam46a* (XM_005157860.2), *npvf* (NM_001082949.1), *npffr* (NM_001171697.1), *zgc:171844* (NM_001127478.1), *hmx3* (NM_131634.1), *lhx9* (NM_001017710.1), *si:dkey-58b18.8* (ENSDARG00000095761), *elovl7b* (NM_199778.1), *gad67* (NM_194419.1), *vglut2b* (NM_001009982.1), *hsf1* (NM_131600.1) and *cuff23873*. All PCR products were cloned into a pCRII-TOPO vector (Invitrogen, Carlsbad, CA) and served as a template to transcribe digoxigenin-labeled antisense mRNA probes.

***In-situ* hybridization.** Larvae and adult brains were fixed in 4% paraformaldehyde over 48 h at 4ºC. All samples were then dehydrated in 100% methanol and stored at -20ºC. Before further treatment, brains and larvae were rehydrated in decreasing methanol concentrations. Adult brains were embedded in 2.5% agarose and sectioned with the Vibratome Series 1000 Sectioning System (Campden Instruments, Lafayette, IN). Transverse sections were then processed and stained as free-floating slices. ISH was performed following standard protocols. Digoxigenin-

and fluorescein-labeled antisense riboprobes were transcribed *in vitro* using RNA Labeling Kit SP6/T7 (Roche Diagnostics Corporation, Indianapolis, IN). Single probe ISH was revealed with colorimetric BM purple (Roche Diagnostics Corporation, Indianapolis, IN). Double probe fluorescent ISH was performed as described previously (101)

Fluorescent ISH and immunofluorescence staining. ISH was performed as described above in *hcrt:EGFP* 2 dpf larvae and adults. The samples were revealed using Fast Red (Roche Diagnostics Corporation, Indianapolis, IN). All the procedures were based on standard protocols (101). After blocking, larvae and adult brain slices were incubated in primary rabbit anti-EGFP (Santa Cruz Biotechnology, Santa Cruz, CA), diluted 1:250. Anti-EGFP antibodies were detected with a secondary goat anti-rabbit Alexa Fluor 488 IgG (H+L) antibody (2 mg/mL, A-11034, Invitrogen, Carlsbad, CA). All experiments were repeated in 3-5 larvae and adult sections.

Imaging. An epifluorescence stereomicroscope (Leica M165FC) was used to visualize live larvae expressing EGFP and fluorescent-fixed larvae and adult brain sections. Pictures were taken using the Leica Application Suite imaging software, version 3.7 (Leica, Wetzlar, Germany). In confocal imaging of fixed embryos, the samples were mounted on slides. In live imaging of *hcrt:EGFP* larvae, the larvae were mounted in low-melting–point 1% agarose. Confocal imaging was performed using a Zeiss LSM710 upright confocal microscope (Zeiss, Oberkochen, Germany). All images were processed using ImageJ (National Institutes of Health, Bethesda, MD).

Establishment of a *kcnh4a* mutant (*kcnh4a*$^{-/-}$) line. The CRISPR system (102) was used to establish the *kcnh4a*$^{-/-}$ line. The Cas9 (Addgene plasmid no. 42251) and sgRNA (Addgene plasmid no. DR274) zebrafish expression plasmids were obtained from Addgene (Cambridge, MA). In order to prepare the sgRNA, two *kcnh4a*-specific oligos were designed to match the target site (ACAACGTCTGCTTCTCCACCC) in exon 5. These oligos were denatured at 95^{o}C for 5 min, then gradually cooled down to room temperature and kept at 4^{o}C. Before cloning, annealing of the oligos was confirmed in 2% agarose gel. The annealed oligos were cloned into the DR274 plasmid between the *BsaI* restriction sites and transformed into bacteria, which was selected by standard sequencing. In order to synthesize the specific sgRNA, the DR274 plasmid containing the annealed oligos was linearized with the restriction enzyme *DraI*, and cleaned using the standard phenol-chloroform procedure, followed by purification by the PureLink PCR Purification Kit (#K31000, Life Technologies, Carlsbad, CA). The sgRNA was synthesized using the T7 High Yield RNA Synthesis Kit (New England Biolabs, Hitchin, UK). In order to prepare *Cas9* mRNA, the zebrafish Cas9 vector was linearized by *AgeI*, and mRNA was synthesized using the mMESSAGE mMACHINE T7 Kit (Life Technologies, Carlsbad, CA).

One-cell–stage WT zebrafish embryos were microinjected with mixed *Cas9* mRNA (300 ng/µl) and transcribed sgRNA (12.5 ng/µl). To test the efficiency of the CRISPR system, ten 1-dpf embryos were screened for *kcnh4a*-specific mutation (as described below). We found that 60% of the embryos carried the mutation. The founder (F0) mosaic embryos were raised to adulthood and outcrossed with WT fish in order to identify F1 mutant fish. Single F1 heterozygous fish, which carry a 14 bp

deletion mutation in the *kcnh4a* target site (Figure 6D), was selected and outcrossed with WT fish. To decrease the risk for off-target mutations, heterozygous F2 and then F3 fish were outcrossed with WT fish. In all experiments, heterozygous F4 fish were intercrossed, and the assays were performed on their progeny.

Genotyping. Genotyping of the *kcnh4a*$^{-/-}$ zebrafish was conducted by extracting genomic DNA from embryos and larvae or by the tail clipping of adult fish using the KAPA Express Extract Kit (Kapa Biosystems Inc., Boston, MA) according to the manufacturer's instructions. Genomic DNA was then amplified by PCR using the following primers: forward- 5'TTCATGTTTTCCACAGAATGTGTTTTCACA3' and reverse- 5'ACCGAGGATGAAGAGCATCTCCACAG3'. The PCR product was then run on 2% agarose gel, and heterozygous, homozygous, and WT fragments could be identified by their size (Figure 6D). To confirm the gel pattern, selected PCR products were sequenced.

Behavioral assays. The *kcnh4a*$^{+/-}$ adult zebrafish were intercrossed and their progeny were kept under LD cycle. At 5 dpf, the larvae were individually placed in 48-well plates. At 6 dpf, larva-containing plates were placed in the Noldus DanioVision tracking system (Noldus Information Technology, Wageningen, Netherlands) and acclimated for one hour prior to behavioral recording. Recording was performed using the EthoVision XT 9 software (Noldus Information Technology, Wageningen, Netherlands), as previously described (48). Light intensity in the tracking system was 70 LUX for all experiments. To monitor rhythmic behavior during a daily cycle, larvae were maintained under the LD cycle, which was similar to the LD cycle prior to the experiment. Data analyses of total locomotor activity,

sleep time, sleep/wake transitions, and sleep-bout length were performed according to the parameters previously described (48). Following each behavioral experiment, all larvae were subject to genotyping (as described above). SD was performed by randomized manual tapping on a petri dish that contained 6 dpf larvae. Following the SD, sleep time was monitored in sleep-deprived and control larvae (n=13 for each treatment) using behavioral systems.

Statistical analysis. In the RNA-seq data, statistically significant differences between the number of reads aligned to each gene (the expression profile) in the different tested conditions, without unifying the replicates, were identified as previously described (103,104). Briefly, the expression profiles were normalized using a variation of the trimmed mean of M-values normalization method (104,105). Subsequently, we searched for expression differences between the $EGFP^+$ and the control samples that cannot be explained by Poisson noise with $p < 0.01$ and Bonferroni correction for multiple testing (104). Notably, the analysis takes into account technical biases that can cause the variance to be larger than that of naive Poisson statistics (104). Only genes with average expression >15 (raw reads) in the $EGFP^+$ samples were analyzed, and only genes with fold change higher than 3.6 are shown in Figure 2–source data 1.

In the behavioral experiments, statistical analysis was performed using SAS v9.3 software (SAS Institute, Cary, NC). Locomotor activity, sleep time, sleep-bout length, and sleep/wake transitions were analyzed with repeated measures of ANOVA (SAS PROC MIXED), where each was modeled as a function of genotype (*kcnh4a*$^{-/-}$, *kcnh4a*$^{+/-}$, *kcnh4a*$^{+/+}$), time (24 h), and the genotype by time interaction term. LS means (model estimated means) differences between the genotype groups

per time point were estimated from the model interaction terms and are presented with respective levels of significance and 95% confidence intervals. These were used to compare between genotypes per time point in locomotor activity and sleep experiments.

Acknowledgments

This work was supported by the US-Israel Binational Science Foundation (Grant number 2011335), the Israel Science Foundation (Grant number 366/11), the Legacy Heritage Biomedical Program of the Israel Science Foundation (Grant numbers 398/11 and 992/14), and Marie Curie Actions-International Reintegration (Grant number FP7-PEOPLE-2010-RG274333). We thank the Appelbaum lab members Adi Tovin, Adi Shamay-Ramot, David Zada, and Tali Levitas-Djerbi for technical assistance and helpful comments. We thank Karina Yaniv (Weizmann Institute of Science, Israel) for helping with the FACS experiments. We thank Sharon Victor for assistance in English editing of the manuscript and Lisa Deutsch for performing statistical analyses of the data.

References

1. Shepard JW, Buysse DJ, Chesson AL, Dement WC, Goldberg R, Guilleminault C, et al. History of the development of sleep medicine in the United States. J Clin Sleep Med JCSM Off Publ Am Acad Sleep Med. 2005 Jan 15;1:61–82.

2. Begg DP, Woods SC. The endocrinology of food intake. Nat Rev Endocrinol. 2013 Oct;9:584–97.

3. Dietrich MO, Horvath TL. Hypothalamic control of energy balance: insights into the role of synaptic plasticity. Trends Neurosci. 2013 Feb;36:65–73.

4. Mignot E, Taheri S, Nishino S. Sleeping with the hypothalamus: emerging therapeutic targets for sleep disorders. Nat Neurosci. 2002 Nov;5 Suppl:1071–5.

5. Muindi F, Zeitzer JM, Heller HC. Retino-hypothalamic regulation of light-induced murine sleep. Front Syst Neurosci. 2014;8:135.

6. Salin-Pascual R, Gerashchenko D, Greco M, Blanco-Centurion C, Shiromani PJ. Hypothalamic regulation of sleep. Neuropsychopharmacol Off Publ Am Coll Neuropsychopharmacol. 2001 Nov;25:S21–7.

7. Saper CB. Staying awake for dinner: hypothalamic integration of sleep, feeding, and circadian rhythms. Prog Brain Res. 2006;153:243–52.

8. Saper CB, Scammell TE, Lu J. Hypothalamic regulation of sleep and circadian rhythms. Nature. 2005 Oct 27;437:1257–63.

9. Sternson SM. Hypothalamic survival circuits: blueprints for purposive behaviors. Neuron. 2013 Mar 6;77:810–24.

10. Welsh DK, Takahashi JS, Kay SA. Suprachiasmatic nucleus: cell autonomy and network properties. Annu Rev Physiol. 2010;72:551–77.

11. Dietrich MO, Horvath TL. Limitations in anti-obesity drug development: the critical role of hunger-promoting neurons. Nat Rev Drug Discov. 2012 Sep;11:675–91.

12. Rolls A, Schaich Borg J, de Lecea L. Sleep and metabolism: role of hypothalamic neuronal circuitry. Best Pract Res Clin Endocrinol Metab. 2010 Oct;24:817–28.

13. Sakurai T, Mieda M. Connectomics of orexin-producing neurons: interface of systems of emotion, energy homeostasis and arousal. Trends Pharmacol Sci. 2011 Aug;32:451–62.

14. Sakurai T. The neural circuit of orexin (hypocretin): maintaining sleep and wakefulness. Nat Rev Neurosci. 2007 Mar;8:171–81.

15. de Lecea L, Kilduff TS, Peyron C, Gao X, Foye PE, Danielson PE, et al. The hypocretins: hypothalamus-specific peptides with neuroexcitatory activity. Proc Natl Acad Sci U S A. 1998 Jan 6;95:322–7.

16. Sakurai T, Amemiya A, Ishii M, Matsuzaki I, Chemelli RM, Tanaka H, et al. Orexins and orexin receptors: a family of hypothalamic neuropeptides and G protein-coupled receptors that regulate feeding behavior. Cell. 1998 Feb 20;92:573–85.

17. Adamantidis AR, Zhang F, Aravanis AM, Deisseroth K, de Lecea L. Neural substrates of awakening probed with optogenetic control of hypocretin neurons. Nature. 2007 Nov 15;450:420–4.

18. Burgess CR, Scammell TE. Narcolepsy: neural mechanisms of sleepiness and cataplexy. J Neurosci Off J Soc Neurosci. 2012 Sep 5;32:12305–11.

19. Chemelli RM, Willie JT, Sinton CM, Elmquist JK, Scammell T, Lee C, et al. Narcolepsy in orexin knockout mice: molecular genetics of sleep regulation. Cell. 1999 Aug 20;98:437–51.

20. Lin L, Faraco J, Li R, Kadotani H, Rogers W, Lin X, et al. The sleep disorder canine narcolepsy is caused by a mutation in the hypocretin (orexin) receptor 2 gene. Cell. 1999 Aug 6;98:365–76.

21. Peyron C, Faraco J, Rogers W, Ripley B, Overeem S, Charnay Y, et al. A mutation in a case of early onset narcolepsy and a generalized absence of hypocretin peptides in human narcoleptic brains. Nat Med. 2000 Sep;6:991–7.

22. Schuld A, Hebebrand J, Geller F, Pollmacher T. Increased body-mass index in patients with narcolepsy. Lancet. 2000 Apr 8;355:1274–5.

23. Boutrel B, Steiner N, Halfon O. The hypocretins and the reward function: what have we learned so far? Front Behav Neurosci. 2013;7:59.

24. Tsujino N, Sakurai T. Role of orexin in modulating arousal, feeding, and motivation. Front Behav Neurosci. 2013;7:28.

25. Henny P, Brischoux F, Mainville L, Stroh T, Jones BE. Immunohistochemical evidence for synaptic release of glutamate from orexin terminals in the locus coeruleus. Neuroscience. 2010 Sep 1;169:1150–7.

26. Schone C, Cao ZF, Apergis-Schoute J, Adamantidis A, Sakurai T, Burdakov D. Optogenetic probing of fast glutamatergic transmission from hypocretin/orexin to histamine neurons in situ. J Neurosci Off J Soc Neurosci. 2012 Sep 5;32:12437–43.

27. Appelbaum L, Skariah G, Mourrain P, Mignot E. Comparative expression of p2x receptors and ecto-nucleoside triphosphate diphosphohydrolase 3 in hypocretin and sensory neurons in zebrafish. Brain Res. 2007 Oct 12;1174:66–75.

28. Appelbaum L, Wang G, Yokogawa T, Skariah GM, Smith SJ, Mourrain P, et al. Circadian and homeostatic regulation of structural synaptic plasticity in hypocretin neurons. Neuron. 2010 Oct 6;68:87–98.

29. Belcher SM, Zsarnovszky A, Crawford PA, Hemani H, Spurling L, Kirley TL. Immunolocalization of ecto-nucleoside triphosphate diphosphohydrolase 3 in rat brain: implications for modulation of multiple homeostatic systems including feeding and sleep-wake behaviors. Neuroscience. 2006;137:1331–46.

30. Blouin AM, Thannickal TC, Worley PF, Baraban JM, Reti IM, Siegel JM. Narp immunostaining of human hypocretin (orexin) neurons: loss in narcolepsy. Neurology. 2005 Oct 25;65:1189–92.

31. Broberger C. Hypothalamic cocaine- and amphetamine-regulated transcript (CART) neurons: histochemical relationship to thyrotropin-releasing hormone, melanin-concentrating hormone, orexin/hypocretin and neuropeptide Y. Brain Res. 1999 Nov 27;848:101–13.

32. Crocker A, Espana RA, Papadopoulou M, Saper CB, Faraco J, Sakurai T, et al. Concomitant loss of dynorphin, NARP, and orexin in narcolepsy. Neurology. 2005 Oct 25;65:1184–8.

33. Cvetkovic-Lopes V, Bayer L, Dorsaz S, Maret S, Pradervand S, Dauvilliers Y, et al. Elevated Tribbles homolog 2-specific antibody levels in narcolepsy patients. J Clin Invest. 2010 Mar 1;120:713–9.

34. Dalal J, Roh JH, Maloney SE, Akuffo A, Shah S, Yuan H, et al. Translational profiling of hypocretin neurons identifies candidate molecules for sleep regulation. Genes Dev. 2013 Mar 1;27:565–78.

35. Florenzano F, Viscomi MT, Mercaldo V, Longone P, Bernardi G, Bagni C, et al. P2X2R purinergic receptor subunit mRNA and protein are expressed by all hypothalamic hypocretin/orexin neurons. J Comp Neurol. 2006 Sep 1;498:58–67.

36. Honda M, Eriksson KS, Zhang S, Tanaka S, Lin L, Salehi A, et al. IGFBP3 colocalizes with and regulates hypocretin (orexin). PloS One. 2009;4:e4254.

37. Liu J, Merkle FT, Gandhi AV, Gagnon JA, Woods IG, Chiu CN, et al. Evolutionarily conserved regulation of hypocretin neuron specification by Lhx9. Development. 2015 Mar 15;142:1113–24.

38. Meister B, Hakansson ML. [Orexins--new hypothalamic peptides that stimulate appetite]. Lakartidningen. 1998 Dec 16;95:5885–7.

39. Reti IM, Reddy R, Worley PF, Baraban JM. Selective expression of Narp, a secreted neuronal pentraxin, in orexin neurons. J Neurochem. 2002 Sep;82:1561–5.

40. Silva JP, von Meyenn F, Howell J, Thorens B, Wolfrum C, Stoffel M. Regulation of adaptive behaviour during fasting by hypothalamic Foxa2. Nature. 2009 Dec 3;462:646–50.

41. Romano SA, Pietri T, Perez-Schuster V, Jouary A, Haudrechy M, Sumbre G. Spontaneous Neuronal Network Dynamics Reveal Circuit's Functional Adaptations for Behavior. Neuron. 2015 Feb 17;

42. Severi KE, Portugues R, Marques JC, O'Malley DM, Orger MB, Engert F. Neural control and modulation of swimming speed in the larval zebrafish. Neuron. 2014 Aug 6;83:692–707.

43. Thiele TR, Donovan JC, Baier H. Descending control of swim posture by a midbrain nucleus in zebrafish. Neuron. 2014 Aug 6;83:679–91.

44. Zhdanova IV, Wang SY, Leclair OU, Danilova NP. Melatonin promotes sleep-like state in zebrafish. Brain Res. 2001 Jun 8;903(1-2):263–8.

45. Prober DA, Rihel J, Onah AA, Sung RJ, Schier AF. Hypocretin/orexin overexpression induces an insomnia-like phenotype in zebrafish. J Neurosci Off J Soc Neurosci. 2006 Dec 20;26:13400–10.

46. Yokogawa T, Marin W, Faraco J, Pezeron G, Appelbaum L, Zhang J, et al. Characterization of sleep in zebrafish and insomnia in hypocretin receptor mutants. PLoS Biol. 2007 Oct 16;5:e277.

47. Sigurgeirsson B, Thorsteinsson H, Arnardóttir H, Jóhannesdóttir IT, Karlsson KA. Effects of modafinil on sleep-wake cycles in larval zebrafish. Zebrafish. 2011 Sep;8(3):133–40.

48. Elbaz I, Yelin-Bekerman L, Nicenboim J, Vatine G, Appelbaum L. Genetic ablation of hypocretin neurons alters behavioral state transitions in zebrafish. J Neurosci Off J Soc Neurosci. 2012 Sep 12;32:12961–72.

49. Faraco JH, Appelbaum L, Marin W, Gaus SE, Mourrain P, Mignot E. Regulation of hypocretin (orexin) expression in embryonic zebrafish. J Biol Chem. 2006 Oct 6;281:29753–61.

50. Kaslin J, Nystedt JM, Ostergard M, Peitsaro N, Panula P. The orexin/hypocretin system in zebrafish is connected to the aminergic and cholinergic systems. J Neurosci Off J Soc Neurosci. 2004 Mar 17;24:2678–89.

51. Yokobori E, Kojima K, Azuma M, Kang KS, Maejima S, Uchiyama M, et al. Stimulatory effect of intracerebroventricular administration of orexin A on food intake in the zebrafish, Danio rerio. Peptides. 2011 Jul;32:1357–62.

52. Appelbaum L, Wang GX, Maro GS, Mori R, Tovin A, Marin W, et al. Sleep-wake regulation and hypocretin-melatonin interaction in zebrafish. Proc Natl Acad Sci U S A. 2009 Dec 22;106:21942–7.

53. Perkel JM. Visiting "noncodarnia." BioTechniques. 2013 Jun;54:301, 303–4.

54. Mercer TR, Dinger ME, Mattick JS. Long non-coding RNAs: insights into functions. Nat Rev Genet. 2009 Mar;10:155–9.

55. Tanaka S, Kodama T, Nonaka T, Toyoda H, Arai M, Fukazawa M, et al. Transcriptional regulation of the hypocretin/orexin gene by NR6A1. Biochem Biophys Res Commun. 2010 Dec 10;403(2):178–83.

56. Santos SD, Saraiva MJ. Enlarged ventricles, astrogliosis and neurodegeneration in heat shock factor 1 null mouse brain. Neuroscience. 2004;126:657–63.

57. Tucker NR, Middleton RC, Le QP, Shelden EA. HSF1 is essential for the resistance of zebrafish eye and brain tissues to hypoxia/reperfusion injury. PloS One. 2011;6:e22268.

58. Chakravarthy MV, Lodhi IJ, Yin L, Malapaka RR, Xu HE, Turk J, et al. Identification of a physiologically relevant endogenous ligand for PPARalpha in liver. Cell. 2009 Aug 7;138:476–88.

59. Fu J, Gaetani S, Oveisi F, Lo Verme J, Serrano A, Rodriguez De Fonseca F, et al. Oleylethanolamide regulates feeding and body weight through activation of the nuclear receptor PPAR-alpha. Nature. 2003 Sep 4;425:90–3.

60. Kops GJ, de Ruiter ND, De Vries-Smits AM, Powell DR, Bos JL, Burgering BM. Direct control of the Forkhead transcription factor AFX by protein kinase B. Nature. 1999 Apr 15;398:630–4.

61. Plengvidhya N, Kooptiwut S, Songtawee N, Doi A, Furuta H, Nishi M, et al. PAX4 mutations in Thais with maturity onset diabetes of the young. J Clin Endocrinol Metab. 2007 Jul;92:2821–6.

62. Reiner AP, Gross MD, Carlson CS, Bielinski SJ, Lange LA, Fornage M, et al. Common coding variants of the HNF1A gene are associated with multiple cardiovascular risk phenotypes in community-based samples of younger and older European-American adults: the Coronary Artery Risk Development in Young Adults Study and The Cardiovascular Health Study. Circ Cardiovasc Genet. 2009 Jun;2:244–54.

63. Schmutz I, Ripperger JA, Baeriswyl-Aebischer S, Albrecht U. The mammalian clock component PERIOD2 coordinates circadian output by interaction with nuclear receptors. Genes Dev. 2010 Feb 15;24:345–57.

64. Turek M, Lewandrowski I, Bringmann H. An AP2 transcription factor is required for a sleep-active neuron to induce sleep-like quiescence in C. elegans. Curr Biol CB. 2013 Nov 18;23:2215–23.

65. Choe S. Potassium channel structures. Nat Rev Neurosci. 2002 Feb;3:115–21.

66. Bezanilla F. The voltage sensor in voltage-dependent ion channels. Physiol Rev. 2000 Apr;80:555–92.

67. Swartz KJ. Sensing voltage across lipid membranes. Nature. 2008 Dec 18;456:891–7.

68. Dereeper A, Guignon V, Blanc G, Audic S, Buffet S, Chevenet F, et al. Phylogeny.fr: robust phylogenetic analysis for the non-specialist. Nucleic Acids Res. 2008 Jul 1;36:W465–9.

69. Zhdanova IV. Sleep and its regulation in zebrafish. Rev Neurosci. 2011;22(1):27–36.

70. Elbaz I, Foulkes NS, Gothilf Y, Appelbaum L. Circadian clocks, rhythmic synaptic plasticity and the sleep-wake cycle in zebrafish. Front Neural Circuits. 2013;7:9.

71. Choe S. Potassium channel structures. Nat Rev Neurosci. 2002 Feb;3:115–21.

72. Primo ME, Klinke S, Sica MP, Goldbaum FA, Jakoncic J, Poskus E, et al. Structure of the mature ectodomain of the human receptor-type protein-tyrosine phosphatase IA-2. J Biol Chem. 2008 Feb 22;283:4674–81.

73. Saito H. Structural diversity of eukaryotic protein tyrosine phosphatases: functional and evolutionary implications. Semin Cell Biol. 1993 Dec;4:379–87.

74. Funder JW, Krozowski Z, Myles K, Sato A, Sheppard KE, Young M. Mineralocorticoid receptors, salt, and hypertension. Recent Prog Horm Res. 1997;52:247–60; discussion 261–2.

75. Ings JS, Van Der Kraak GJ. Characterization of the mRNA expression of StAR and steroidogenic enzymes in zebrafish ovarian follicles. Mol Reprod Dev. 2006 Aug;73:943–54.

76. Stocco DM, Wang X, Jo Y, Manna PR. Multiple signaling pathways regulating steroidogenesis and steroidogenic acute regulatory protein expression: more complicated than we thought. Mol Endocrinol. 2005 Nov;19:2647–59.

77. Brolinson A, Fourcade S, Jakobsson A, Pujol A, Jacobsson A. Steroid hormones control circadian Elovl3 expression in mouse liver. Endocrinology. 2008 Jun;149:3158–66.

78. Chen YS, Luo WI, Lee TL, Yu SS, Chang CY. Identification of the proteins required for fatty acid desaturation in zebrafish (Danio rerio). Biochem Biophys Res Commun. 2013 Nov 1;440:671–6.

79. Craxton M. A manual collection of Syt, Esyt, Rph3a, Rph3al, Doc2, and Dblc2 genes from 46 metazoan genomes--an open access resource for neuroscience and evolutionary biology. BMC Genomics. 2010;11:37.

80. Zhao E, Li Y, Fu X, Zeng L, Zeng H, Jin W, et al. Cloning and characterization of human synaptotagmin 10 gene. DNA Seq J DNA Seq Mapp. 2003 Oct;14:393–8.

81. Sager C, Tapken D, Kott S, Hollmann M. Functional modulation of AMPA receptors by transmembrane AMPA receptor regulatory proteins. Neuroscience. 2009 Jan 12;158:45–54.

82. Fischer-Colbrie R, Kirchmair R, Kahler CM, Wiedermann CJ, Saria A. Secretoneurin: a new player in angiogenesis and chemotaxis linking nerves, blood vessels and the immune system. Curr Protein Pept Sci. 2005 Aug;6:373–85.

83. Kassahn KS, Dang VT, Wilkins SJ, Perkins AC, Ragan MA. Evolution of gene function and regulatory control after whole-genome duplication: comparative analyses in vertebrates. Genome Res. 2009 Aug;19:1404–18.

84. Wu X, Bradley MJ, Cai Y, Kummel D, De La Cruz EM, Barr FA, et al. Insights regarding guanine nucleotide exchange from the structure of a DENN-domain protein complexed with its Rab GTPase substrate. Proc Natl Acad Sci U S A. 2011 Nov 15;108:18672–7.

85. Nakashiba T, Ikeda T, Nishimura S, Tashiro K, Honjo T, Culotti JG, et al. Netrin-G1: a novel glycosyl phosphatidylinositol-linked mammalian netrin that is functionally divergent from classical netrins. J Neurosci Off J Soc Neurosci. 2000 Sep 1;20:6540–50.

86. Seo JS, Kim MS, Park EM, Ahn SJ, Kim NY, Jung SH, et al. Cloning and characterization of muscarinic receptor genes from the nile tilapia (Oreochromis niloticus). Mol Cells. 2009 Mar 31;27:383–90.

87. Goodrich JA, Kugel JF. Non-coding-RNA regulators of RNA polymerase II transcription. Nat Rev Mol Cell Biol. 2006 Aug;7:612–6.

88. Liu Q, Guan XM, Martin WJ, McDonald TP, Clements MK, Jiang Q, et al. Identification and characterization of novel mammalian neuropeptide FF-like peptides that attenuate morphine-induced antinociception. J Biol Chem. 2001 Oct 5;276:36961–9.

89. Delaney G, Dawe KL, Hogan R, Hunjan T, Roper J, Hazell G, et al. Role of nociceptin/orphanin FQ and NOP receptors in the response to acute and repeated restraint stress in rats. J Neuroendocrinol. 2012 Dec;24:1527–41.

90. Xie X, Wisor JP, Hara J, Crowder TL, LeWinter R, Khroyan TV, et al. Hypocretin/orexin and nociceptin/orphanin FQ coordinately regulate analgesia in a mouse model of stress-induced analgesia. J Clin Invest. 2008 Jul;118:2471–81.

91. Rihel J, Prober DA, Arvanites A, Lam K, Zimmerman S, Jang S, et al. Zebrafish behavioral profiling links drugs to biological targets and rest/wake regulation. Science. 2010 Jan 15;327:348–51.

92. Cirelli C, Bushey D, Hill S, Huber R, Kreber R, Ganetzky B, et al. Reduced sleep in Drosophila Shaker mutants. Nature. 2005 Apr 28;434:1087–92.

93. Douglas CL, Vyazovskiy V, Southard T, Chiu SY, Messing A, Tononi G, et al. Sleep in Kcna2 knockout mice. BMC Biol. 2007;5:42.

94. Huang H, Ghosh P, van den Pol AN. Prefrontal cortex-projecting glutamatergic thalamic paraventricular nucleus-excited by hypocretin: a feedforward circuit that may enhance cognitive arousal. J Neurophysiol. 2006 Mar;95:1656–68.

95. Carter ME, Yizhar O, Chikahisa S, Nguyen H, Adamantidis A, Nishino S, et al. Tuning arousal with optogenetic modulation of locus coeruleus neurons. Nat Neurosci. 2010 Dec;13:1526–33.

96. Mahlios J, De la Herran-Arita AK, Mignot E. The autoimmune basis of narcolepsy. Curr Opin Neurobiol. 2013 Oct;23:767–73.

97. Trapnell C, Williams BA, Pertea G, Mortazavi A, Kwan G, van Baren MJ, et al. Transcript assembly and quantification by RNA-Seq reveals unannotated transcripts and isoform switching during cell differentiation. Nat Biotechnol. 2010 May;28:511–5.

98. Trapnell C, Roberts A, Goff L, Pertea G, Kim D, Kelley DR, et al. Differential gene and transcript expression analysis of RNA-seq experiments with TopHat and Cufflinks. Nat Protoc. 2012 Mar;7:562–78.

99. Tang R, Dodd A, Lai D, McNabb WC, Love DR. Validation of zebrafish (Danio rerio) reference genes for quantitative real-time RT-PCR normalization. Acta Biochim Biophys Sin. 2007 May;39(5):384–90.

100. Schmittgen TD, Livak KJ. Analyzing real-time PCR data by the comparative C(T) method. Nat Protoc. 2008;3(6):1101–8.

101. Levitas-Djerbi T, Yelin-Bekerman L, Lerer-Goldshtein T, Appelbaum L. Hypothalamic leptin-neurotensin-hypocretin neuronal networks in zebrafish. J Comp Neurol. 2015 Apr 1;523:831–48.

102. Hwang WY, Fu Y, Reyon D, Maeder ML, Tsai SQ, Sander JD, et al. Efficient genome editing in zebrafish using a CRISPR-Cas system. Nat Biotechnol. 2013 Mar;31:227–9.

103. Ben-Moshe Z, Alon S, Mracek P, Faigenbloom L, Tovin A, Vatine GD, et al. The light-induced transcriptome of the zebrafish pineal gland reveals complex regulation of the circadian clockwork by light. Nucleic Acids Res. 2014 Apr;42(6):3750–67.

104. Alon S, Vigneault F, Eminaga S, Christodoulou DC, Seidman JG, Church GM, et al. Barcoding bias in high-throughput multiplex sequencing of miRNA. Genome Res. 2011 Sep;21(9):1506–11.

105. Robinson MD, Oshlack A. A scaling normalization method for differential expression analysis of RNA-seq data. Genome Biol. 2010;11(3):R25.

Figure legends

Figure 1. Isolation of Hcrt neurons, RNA-seq, and experimental design. (A) Dorsal view of 6 dpf *hcrt:EGFP* larvae. **(B)** Dorsal view of the hypothalamus region of 6 dpf *hcrt:EGFP* larvae expressing EGFP in Hcrt neurons. **(C)** Cell suspension from the whole head of 6 dpf *hcrt:EGFP* larvae. **(D-G)** The cells were sorted based on size and fluorescence intensity. The fluorescence thresholds (gray curve) were set based on larvae expressing EGFP under the control of α-tubulin promoter (positive control) **(E)** and WT larvae (negative control) **(F)**. Positive EGFP cells (EGFP+) sorted from *hcrt:EGFP* larvae are marked with gray shade **(G)**. **(H)** PCR amplification of hcrt and egfp was performed on cDNA synthesized from EGFP+ and EGFP- cells sorted from *hcrt:EGFP* larvae. **(I)** FAC-sorting yielded two groups of cells: Group I containing EGFP+ and Group II containing EGFP- cells. A third group contained cells from whole head of WT larvae. The cDNA of groups I and II was amplified and the three groups were then subjected to RNA-seq and bioinformatic analysis to obtain a list of Hcrt-neuron–enriched genes.

Figure 2. The expression pattern of selected candidate Hcrt-neuron–specific genes. (A) Table presenting the top 20 Hcrt-enriched transcripts. **(B-M)** Dorsal view of whole-mount ISH-stained 2 dpf WT larvae. Based on the RNA-seq and the bioinformatic analysis, the expression pattern of selected candidate Hcrt-neuron–specific genes was determined. The expression pattern of *hcrt* **(B)** was used for comparison.

Figure 3. Selected candidate genes are expressed in Hcrt neurons. (A-I'') Double fluorescent staining of the candidate genes (red) and EGFP (green) was performed in 2 dpf *hcrt:EGFP* larvae using whole-mount ISH and immunofluorescence, respectively. White arrows indicate representative co-expressing cells. All confocal images show single plane view of 0.5 μM width. **(J-M'')** Double fluorescent ISH and immunofluorescence experiments in brain sections of *hcrt:EGFP* adult zebrafish. Co-localization of candidate genes (red) and EGFP (green) in Hcrt neurons is shown. All images show single plane view of 0.5 μM width.

Figure 4. Candidate genes are expressed in cell populations located adjacent to Hcrt neurons. (A-I'') Fluorescent ISH and immunofluorescence experiments in 2 dpf larvae and adult *hcrt:EGFP* zebrafish showing three candidate genes that are expressed adjacently to Hcrt neurons within the hypothalamus. **(A-A'', D-D'', G-G'')** Dorsal view of the heads showing the whole expression pattern of the genes in 40 μM z-stack. **(B-B'', E-E'', H-H'')** Dorsal view of single 0.5 μM plane in 2 dpf larvae. **(C-C'', F-F'', I-I'')** Dorsal view of single 0.5 μM plane in adult brain section.

Figure 5. Predicted TFs that regulate the expression of Hcrt-neuron–specific transcripts. (A) TFs with a $p<0.005$ and their target Hcrt-neuron–specific genes. For each of these transcription factors, a combined score for each gene is calculated according to all of the predicted binding sites in its promoter. Therefore, a gene with an overrepresented binding site of a TF will have a high score for that TF and a lower p value. **(B-C'')** Double fluorescent ISH of *hsf1* and immunofluorescence staining of EGFP in *hcrt:EGFP* adult brain section. Single

plane (0.5 μM width) view of the Hcrt-neuron region **(C-C'')**. Arrows mark representative EGFP and *hsf1* co-expressing cell.

Figure 6. The genomic location, phylogenetic reconstruction and structure of *kcnh4a*, and the generation of *kcnh4a-/-* zebrafish. (A) Synteny analysis shows similar genomic context of *hcrt* in zebrafish and mammals. Notably, *kcnh4a* is located a few kbs downstream to *hcrt* in zebrafish and mammals. **(B)** The 16-exon *kcnh4a* gene (black box = exon, white box = UTR) encodes for a voltage-gated potassium channel that includes an N-terminal chain (black bar), pore and voltage-sensing domains (S1-6, grey bar), and the C-terminal chain (red bar). **(C)** A cladogram-style phylogenetic tree depicting the evolutionary conservation of Kcnh4a protein among vertebrates. The tree shows topography as well as distance indicated by the branch support values above corresponding branches. **(D)** Generation of CRISPR-mediated *kcnh4a*$^{-/-}$ zebrafish. A 14 bp deletion was introduced in exon 5 that encodes to the S2 domain. A short mutant allele was visible on agarose gel. **(E)** Quantitative reverse transcription PCR shows reduction of 59% in the expression levels of *kcnh4a* mRNA in *kcnh4a*$^{-/-}$ 6 dpf larvae ($p < 0.001$).

Figure 7. Sleep time and quality are reduced in *kcnh4a-/-* larvae during the night. (A) The locomotor activity of *kcnh4a-/-* (n=85), *kcnh4a+/-* (n=208), and *kcnh4a+/+* (n=98) is shown. *kcnh4a-/-* larvae exhibit increased locomotor activity compared with *kcnh4a+/-* and *kcnh4a+/+* under LD conditions. **(B)** *kcnh4a-/-* larvae showed a significant reduction in sleep time compared with *kcnh4a+/-* and *kcnh4a+/+* during the night. Bar charts represent the average total locomotor activity **(A')** and sleep time **(B')** for each genotype. Values are represented as means±SEM.

(C, D) The number of sleep/wake transitions **(C)** and the length of sleep bout **(D)** are decreased in *kcnh4a*-/- larvae during the night. Recording of locomotor activity and sleep was performed in 6 dpf larvae continuously during 24 h under a 14 h light/10 h dark cycle (white and black bars represent light and dark periods, respectively, **p*<0.05, ***p*<0.01, ****p*<0.0001, with repeated measures of ANOVA).

Figure 2–source data 1. Hcrt-neuron enriched transcripts. All the genes detected have $p < 0.01$ with Bonferroni correction for multiple testing (Methods).

Figure 5–source data 1. Predicted Hcrt-neuron enriched transcription factors and their target genes.

Figure 6–figure supplement 1. Hypothalamic *kcnh4a*-expressing neurons are glutamatergic. Double in-situ hybridization against *kcnh4a* (red, **A**, **B**) and *gad67* (green, **A'**), or *vglut2b* (green, **B'**). All pictures are on a single optical plane of 0.5 µm.

Figure 7–figure supplement 1. Sleep time is increased following sleep deprivation (SD). (A) At 6dpf, larvae were sleep deprived for 6 hours during the night under constant dark conditions (DD) and sleep time was monitored in the following nine hours. **(B, C)** Sleep was recovered in sleep-deprived larvae. Statistical comparisons were performed using Student's t-tests (**p*<0.05). Dark and gray horizontal bars represent night and subjective day, respectively.

Whole head cell dissociation

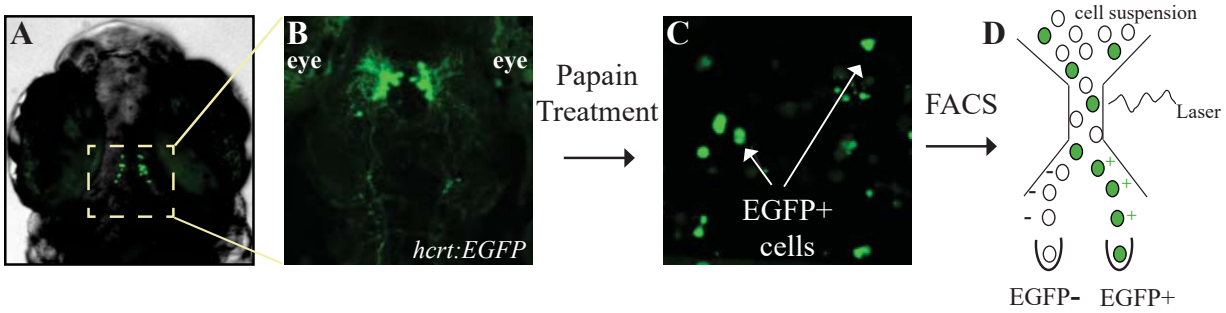

Fluorescence-Activated Cell Sorting of Hcrt neurons

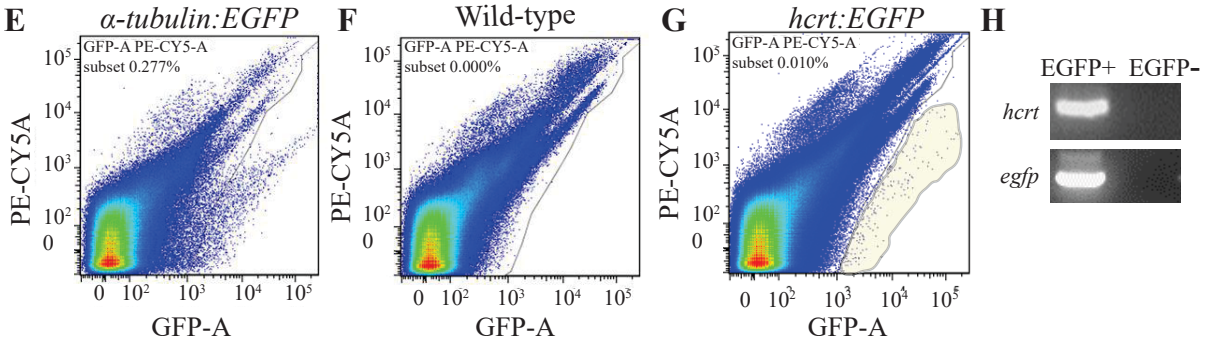

Transcriptome sequencing and bioinformatic analysis

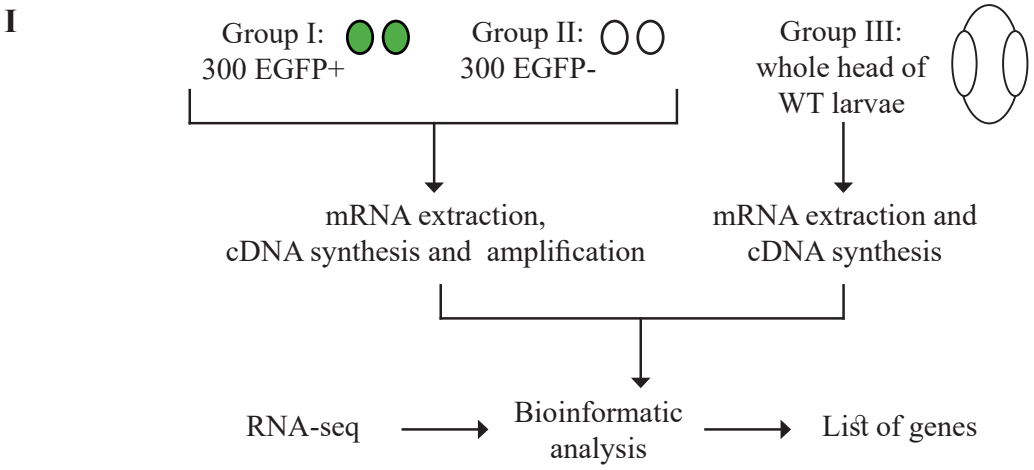

A. Table1: Hcrt-neuron enriched transcripts

Transcript name	Transcript ID	Fold change
npvf	ENSDART00000052627	362.4
hcrt	ENSDART00000104549	54.2
cuff.23873		28.4
cuff.70256		27.9
kcnh4a	ENSDART00000090633	20.2
cuff.64723		15.1
ptgs2b	ENSDART00000010028	14.5
elovl7b	ENSDART00000014385	13.5
cuff.34876		10.8
cuff.57637		10.5
star	ENSDART00000016225	10.5
adra1a	ENSDART00000030938	10.2
grpr	ENSDART00000079150	9.5
cuff.42204		9.3
si:dkey-58b18.8	ENSDART00000144655	8.4
dennd1b	ENSDART00000105614	8.0
cuff.77494		7.9
npffr1l2	ENSDART00000135731	7.5
cuff.77484		7.3
fam46a	ENSDART00000054071	7.2

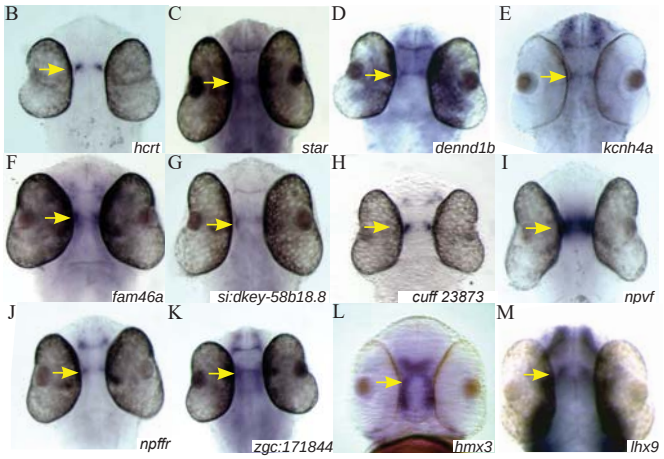

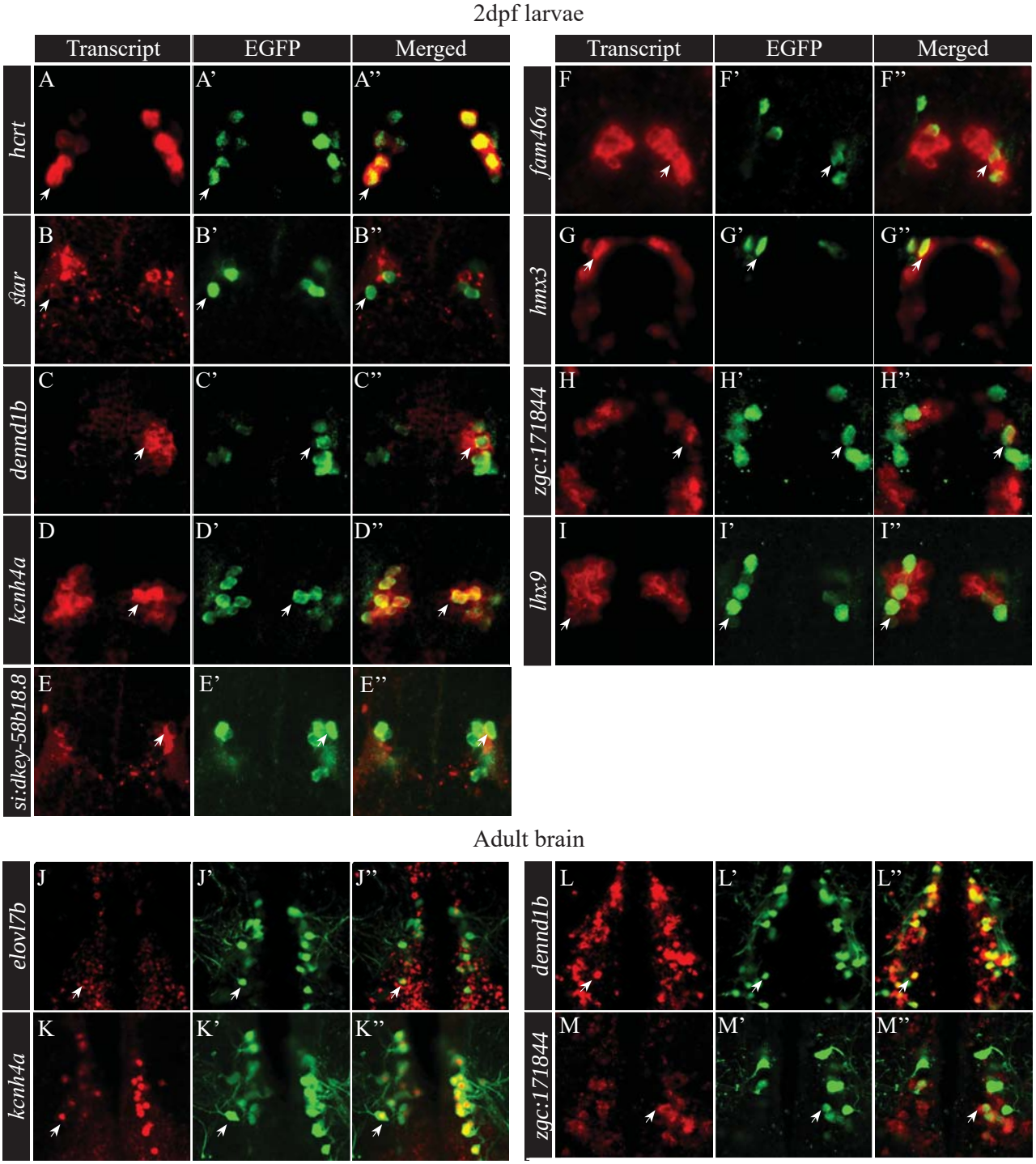
2dpf larvae
Transcript
EGFP
Merged
hcrt
A
A'
A''
star
B
B'
B''
dennd1b
C
C'
C''
kcnh4a
D
D'
D''
si:dkey-58b18.8
E
E'
E''
fam46a
F
F'
F''
hmx3
G
G'
G''
zgc:171844
H
H'
H''
lhx9
I
I'
I''
Adult brain
elovl7b
J
J'
J''
kcnh4a
K
K'
K''
dennd1b
L
L'
L''
zgc:171844
M
M'
M''

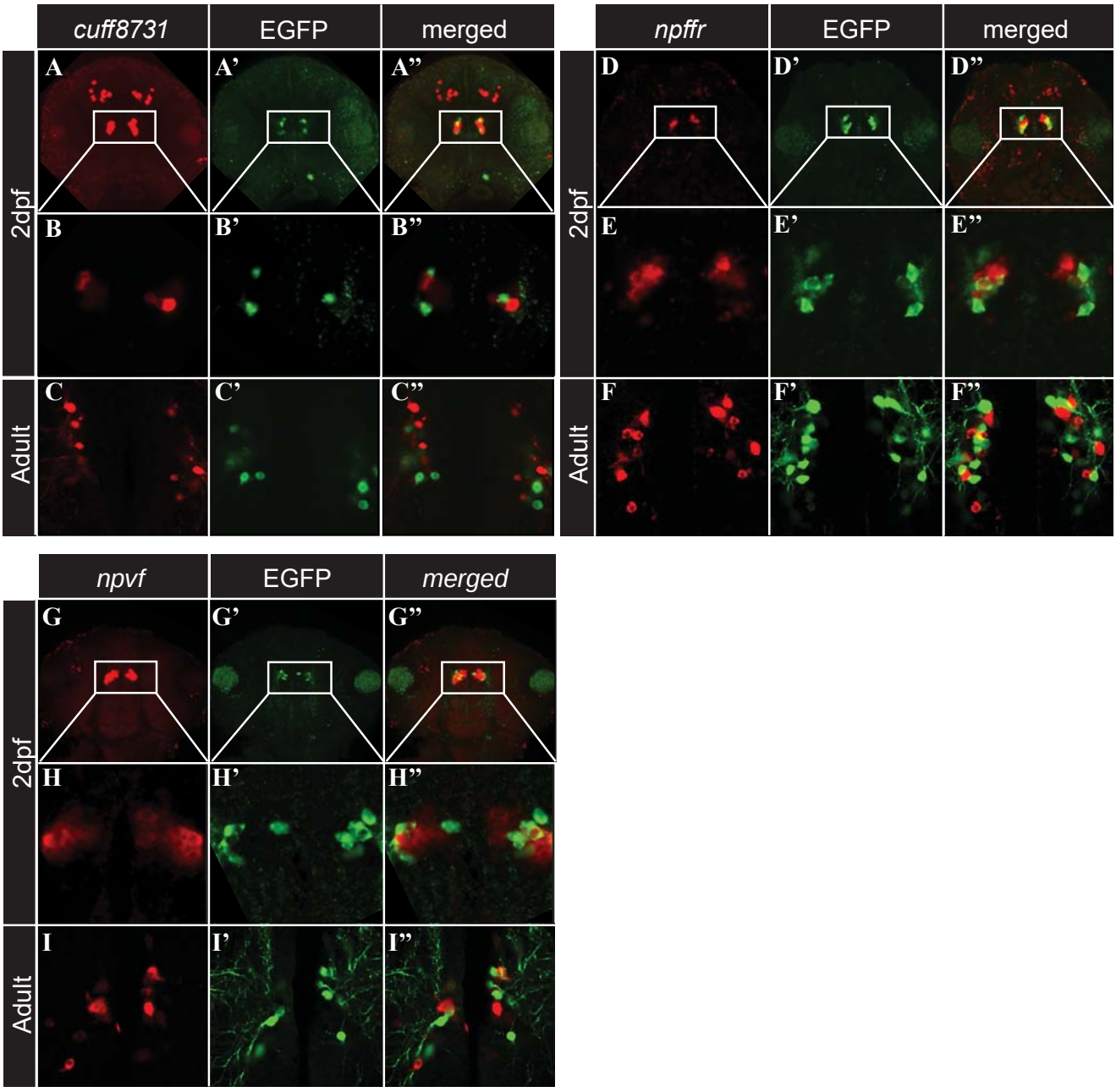
cuff8731
EGFP
merged
npffr
EGFP
merged
npvf
EGFP
merged
2dpf
Adult
A
A'
A"
B
B'
B"
C
C'
C"
D
D'
D"
E
E'
E"
F
F'
F"
G
G'
G"
H
H'
H"
I
I'
I"

A. Predicted Hcrt-neuron enriched transcription factors and their target genes

Transcription factor name	Number of predicted regulated transcripts	*p* <0.005	Predicted regulated transcripts
pax4	44	9.81E-05	*hcrt, ptgs2, fam46a, ttn, pnp, pcsk2, hspa1l, mcoln3, crb1, grpr, creb3l1, elovl7, cetp, krt4, npffr1, slc4a1, lhx9, c16orf45, scg2, soat2, tsen54, nos1, rfx4, syt10, hpcal4, trpc7, ntng1, cacng4, myh4, ptprn, cyb561, epha2, dennd1b, npvf, wscd1, pde2a, adra1a, vgll2, c2cd4a, hmx3, kcnh4a, ugp2, igfbp4, nr5a1*
hsf1	25	1.09E-04	*hcrt, ptgs2, ttn, hspa1l, grpr, elovl7, slc4a1, lhx9, c16orf45, soat2, tsen54, nos1, rfx4, syt10, trpc7, ntng1, cacng4, myh4, dennd1b, sgsm1, pde2a, wscd1, adra1a, kcnh4a, hmx3*
hnf1	35	3.57E-04	*ptgs2, f2rl1, fam46a, ttn, pcsk2, mcoln3, crb1, grpr, creb3l1, elovl7, lhx9, c16orf45, scg2, soat2, nos1, rfx4, syt10, hpcal4, trpc7, ntng1, cacng4, myh4, mmp13, cyb561, epha2, dennd1b, npvf, sgsm1, pde2a, wscd1, adra1a, vgll2, hmx3, ugp2, igfbp4*
ap2	13	4.57E-04	*hcrt, rfx4, ttn, pcsk2, pde2a, wscd1, mcoln3, creb3l1, slc4a1, lhx9, kcnh4a, hmx3, nr5a1*
pou6f1	29	6.29E-04	*star, ptgs2, ttn, fam46a, pnp, pcsk2, mcoln3, crb1, grpr, creb3l1, elovl7, lhx9, c16orf45, syt10, trpc7, ntng1, cacng4, mmp13, cyb561, dennd1b, npvf, sgsm1, adra1a, vgll2, hmx3, ugp2, igfbp4, nr5a1*
ap1	36	8.36E-04	*ttn, pnp, hspa1l, pcsk2, mcoln3, crb1, grpr, creb3l1, elovl7, npffr1, slc4a1, krt4, lhx9, c16orf45, scg2, soat2, nos1, tsen54, rfx4, hpcal4, trpc7, ntng1, cacng4, myh4, ptprn, mmp13, cyb561, epha2, dennd1b, npvf, sgsm1, pde2a, adra1a, nr5a1, igfbp4*
chx10	28	0.001288	*hcrt, ttn, fam46a, pcsk2, crb1, creb3l1, lhx9, scg2, nos1, rfx4, syt10, trpc7, ntng1, cacng4, myh4, cyb561, epha2, dennd1b, npvf, pde2a, wscd1, vgll2, adra1a, hmx3, ugp2, igfbp4, kcnh4a*
ppara	33	0.001779	*hcrt, ptgs2, ttn, fam46a, pnp, hspa1l, pcsk2, crb1, grpr, creb3l1, npffr1, slc4a1, krt4, lhx9, soat2, tsen54, nos1, rfx4, syt10, trpc7, ntng1, cacng4, myh4, ptprn, cyb561, epha2, sgsm1, pde2a, adra1a, hmx3, igfbp4, kcnh4a, nr5a1*
gcnf=nr6a1	34	0.002021	*hcrt, f2rl1, ttn, fam461, pnp, hspa1l, pcsk2, mcoln3, crb1, grpr, creb3l1, slc4a1, npffr1, krt4, scg2, soat2, nos1, rfx4, trpc7, ntng1, cacng4, myh4, ptprn, epha2, dennd1b, npvf, sgsm1, wscd1, pde2a, adra1a, c2cd4a, hmx3, igfbp4, kcmh4a*
mycmax	36	0.00237	*hcrt, star, fam46a, ttn, pnp, pcsk2, hspa1l, crb1, cetp, npffr1, slc4a1, lhx9, c16orf45, scg2, soat2, nos1, rfx4, syt10, hpcal4, trpc7, ntng1, cacng4, myh4, ptprn, cyb561, epha2, dennd1b, npvf, sgsm1, wscd1, pde2a, c2cd4a, hmx3, igfbp4, kcnh4a, nr5a1*
lhx3	25	0.002713	*f2rl1, ttn, fam46a, pcsk2, crb1, grpr, elovl7, lhx9, c16orf45, scg2, nos1, rfx4, syt10, trpc7, ntng1, myh4, cacng4, epha2, dennd1b, npvf, adra1a, c2cd4a, igfbp4, ugp2, nr5a1,*
taxcreb	32	0.003951	*hcrt, f2rl1, ttn, pnp, hspa1l, pcsk2, grpr, creb3l1, npffr1, slc4a1, krt4, tsen54, nos1, rfx4, trpc7, ntng1, cacng4, myh4, ptprn, cyb561, epha2, sgsm1, wscd1, pde2a, adra1a, agll2, c2cd4a, hmx3, ugp2, igfbp4, kcmh4a, nr5a1*
foxo4	32	0.004027	*ptgs2, ttn, fam46a, hspa1l, pcsk2, mcoln3, crb1, grpr, slc4a1, lhx9, c16orf45, soat2, nos1, rfx4, syt10, hpcal4, trpc7, ntng1, cacng4, myh4, ptprn, mmp13, cyb561, dennd1b, sgsm1, wscd1, pde2a, adra1a, c2cd4a, ugp2, igfbp4, nr5a*

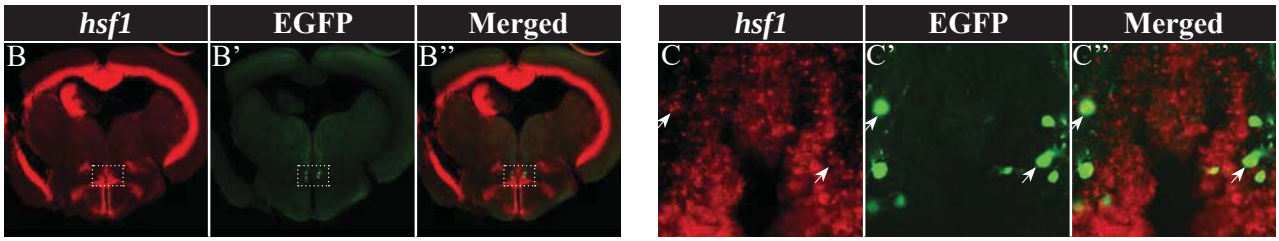

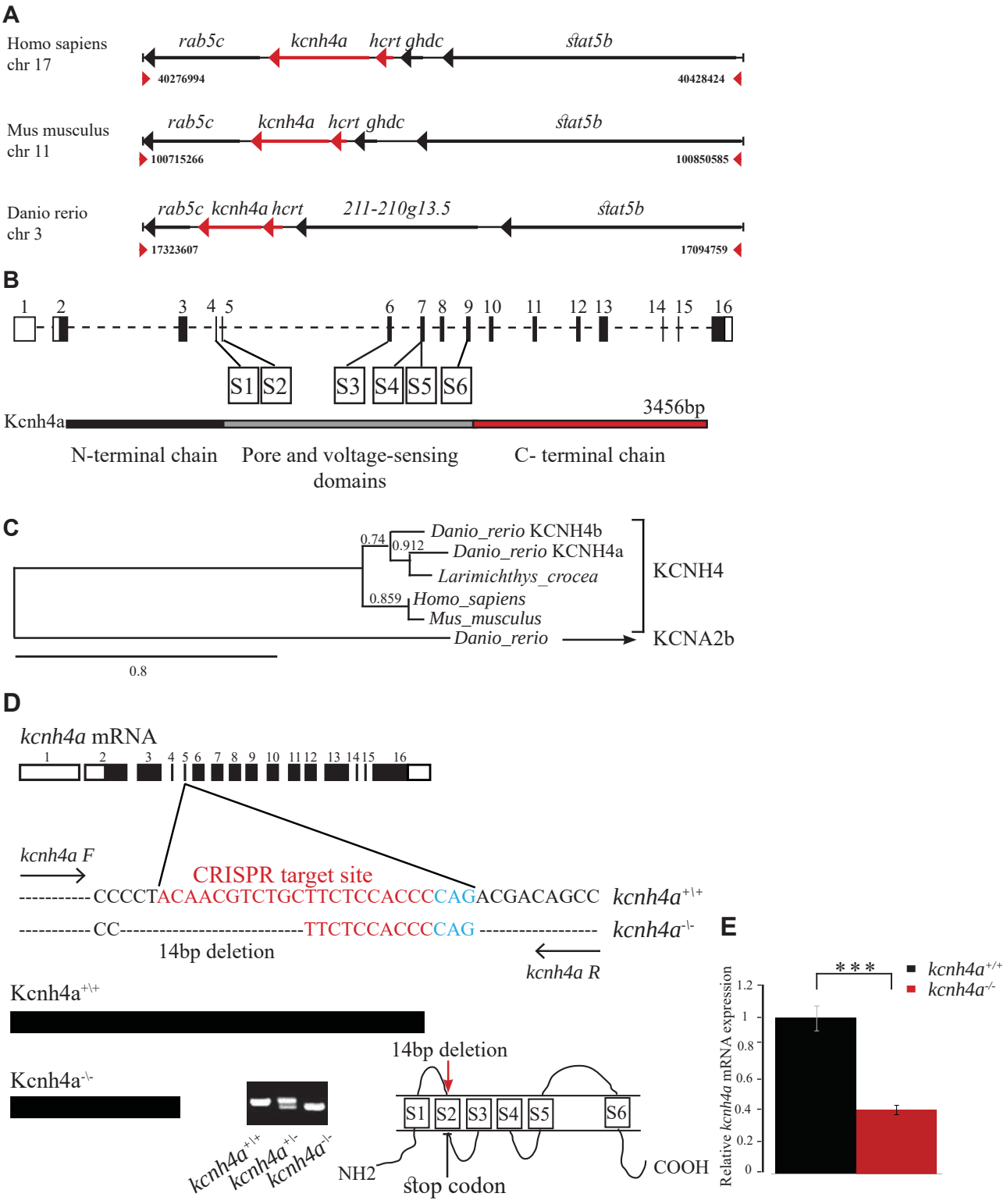
A
Homo sapiens
chr 17
rab5c
kcnh4a
hcrt ghdc
stat5b
40276994
40428424
Mus musculus
chr 11
rab5c
kcnh4a
hcrt ghdc
stat5b
100715266
100850585
Danio rerio
chr 3
rab5c kcnh4a hcrt
211-210g13.5
stat5b
17323607
17094759
B
1 2 3 4 5 6 7 8 9 10 11 12 13 14 15 16
S1 S2 S3 S4 S5 S6
Kcnh4a
3456bp
N-terminal chain
Pore and voltage-sensing domains
C- terminal chain
C
Danio_rerio KCNH4b
Danio_rerio KCNH4a
Larimichthys_crocea
Homo_sapiens
Mus_musculus
Danio_rerio
0.74
0.912
0.859
KCNH4
KCNA2b
0.8
D
kcnh4a mRNA
1 2 3 4 5 6 7 8 9 10 11 12 13 14 15 16
kcnh4a F
CRISPR target site
CCCCTACAACGTCTGCTTCTCCACCCCAGACGACAGCC
kcnh4a+\+
CC
TTCTCCACCCCAG
kcnh4a-\-
14bp deletion
kcnh4a R
Kcnh4a+\+
Kcnh4a-\-
kcnh4a+\+
kcnh4a+\-
kcnh4a-\-
14bp deletion
S1 S2 S3 S4 S5 S6
NH2
COOH
stop codon
E
***
kcnh4a+/+
kcnh4a-/-
Relative kcnh4a mRNA expression
1.2
1
0.8
0.6
0.4
0.2
0

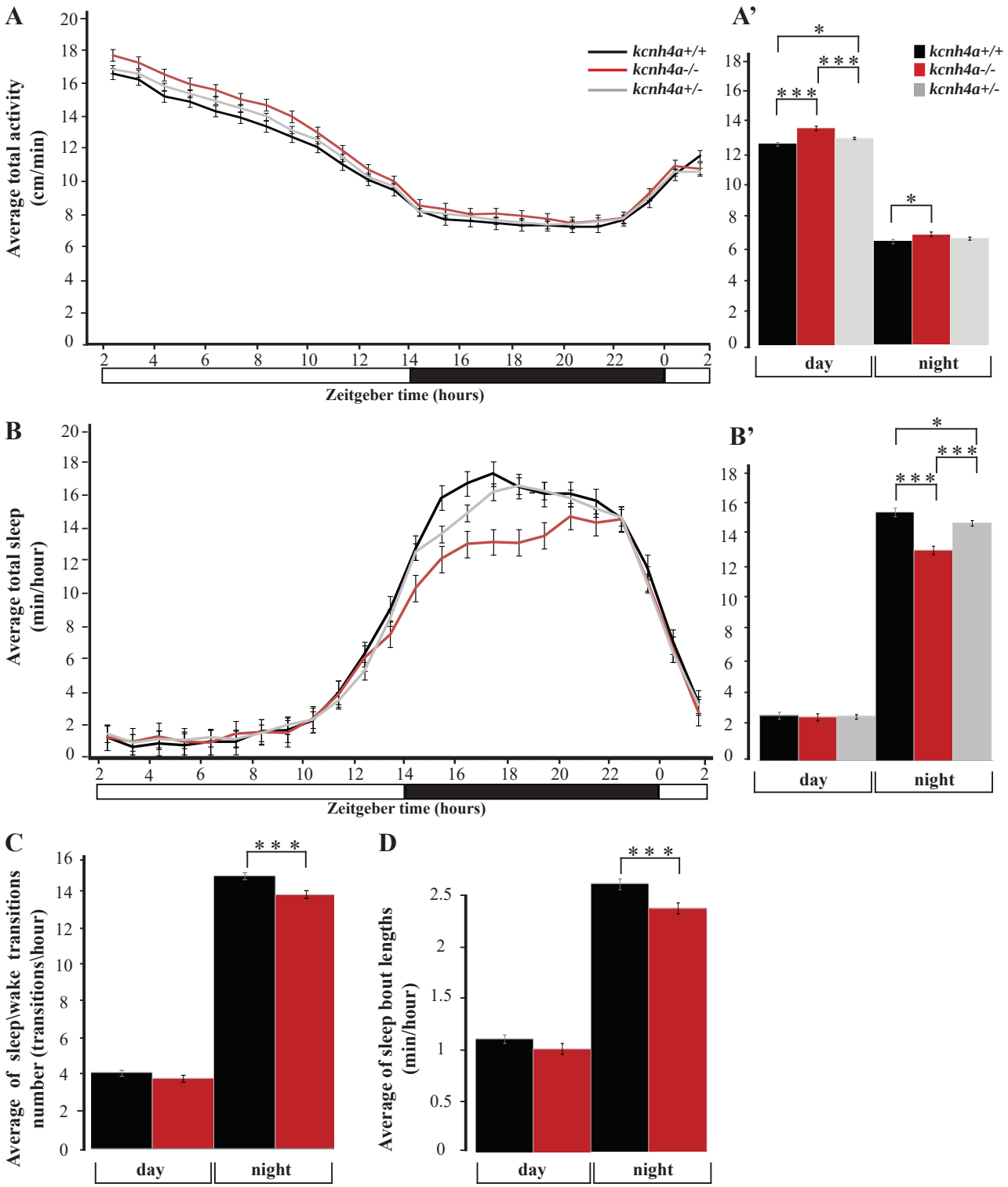
A
Average total activity (cm/min)
kcnh4a+/+
kcnh4a-/-
kcnh4a+/-
Zeitgeber time (hours)
A'
day
night
B
Average total sleep (min/hour)
Zeitgeber time (hours)
B'
C
Average of sleep\wake transitions number (transitions\hour)
D
Average of sleep bout lengths (min/hour)